Quantum Transport: Persistent Current in Mesoscopic Loops

Santanu K. Maiti

Theoretical Condensed Matter Physics Division
Saha Institute of Nuclear Physics
1/AF, Bidhannagar, Kolkata-700 064, India

Electronic Mail: santanu.maiti@saha.ac.in

Contents

A Few Common Symbols

$\vec{A}$	vector potential
B	magnetic field
χ	magnetic susceptibility
D	diffusion coefficient
	Drude weight
e	electronic charge
E	energy
$\mathcal{E}$	electric field
h	Planck's constant
$\hbar$	$= h/2\pi$
H	Hamiltonian
I	current
k_B	Boltzmann constant
L	length
L_ϕ	phase coherence length
N_e	total no. of electrons
μ	electrochemical potential
S	area
T	temperature
τ_ϕ	phase-relaxation time
U	strength of e-e correlation
v_F	Fermi velocity
V	voltage
W	impurity strength

Preface

The physics at submicron length scale, so-called the mesoscopic or nanoscopic physics has seen an enormous evolution over the last two decades both in terms of our understanding of fundamental physics and also in terms of development of revolutionary technologies. The mesoscopic or nanoscopic physics deals with ultrasmall systems where several quantum length scales for the electrons such as system size and phase coherence length, or elastic mean free path and phase coherence length, are comparable. Intense research in this area has revealed the richness of mesoscopic/nanoscopic physics due to the dominance of the quantum effects, which in general can be characterized by an interplay of quantum interference and many-body interaction. The most exotic phenomena are probably the integer and fractional quantum Hall effects, the quantization of conductance through point contact, the Aharonov-Bohm effect, persistent currents in mesoscopic normal metal rings, and single electron charging of quantum dots. In this dissertation we have addressed some issues on electron transport through mesoscopic/nanoscopic systems which are quite challenging.

In a recent experiment Keyser *et al.* [45] have reported the evidence of anomalous Aharonov-Bohm oscillation in the conductance of small quantum rings with few number of electrons. In such small rings with few electrons, electron-electron interaction becomes important as the Coulomb potential is not screened much and we show by exact numerical calculations that similar anomalous oscillation appears in the persistent current due to electron-electron interaction. Our exact calculation leads to several interesting new features of persistent current in the mesoscopic Hubbard rings. The usual saw-tooth behavior of persistent current disappears as we switch on electron-electron interaction. Kink-like structures appear in the persistent current as a function of magnetic flux, and the most interesting result is that the currents inside

the kinks are independent of interaction. The singular behavior of persistent current disappears due to correlation in the half-filled cases with even number of electrons. The mobility of these systems are also determined from the Drude weight, a relevant parameter that characterizes the conducting behavior of the systems. For the metallic phase, Drude weight becomes finite, while it goes to zero in the insulating phase. We observe that for the half-filled systems, mobility of the electrons drops to zero with interaction, while it converges to some finite value for the non-half-filled systems.

A long-standing problem is the anomaly between theory and experiment concerning the amplitudes of persistent currents in the mesoscopic normal metal rings. The measured amplitudes of persistent currents are always one or two orders of magnitude larger than the theoretical estimates. The common notion is that the interplay between disorder and electron-electron interaction plays a very major role in such quantum effects. In a detailed study we show that, electron-electron interaction enhances persistent current in the disordered mesoscopic normal metal rings, but this enhancement is not enough to explain the experimental results. Using a much more realistic model including second neighbor hopping integrals in the usual nearest-neighbor tight-binding Hamiltonian, we get desired enhancement of persistent currents in such systems. We have observed that our model gives the right magnitude of persistent current even in the multi-channel systems which actually corresponds to the experimental situations.

We have also studied the diamagnetic and paramagnetic nature of low-field persistent currents in the mesoscopic rings. In the single-channel perfect rings with both odd and even number of electrons, we get only diamagnetic currents. On the other hand in the single-channel disordered rings, we always have diamagnetic currents with odd number of electrons and paramagnetic currents with even number of electrons. Most interestingly in the multi-channel systems we see that it is not possible to predict precisely the sign of the low-field currents as it strongly depends on the number of electrons and also on the disordered configurations of the system, and the experimental results in fact corroborate this observation.

Topological effects on persistent currents are quite strong in mesoscopic

rings having strip geometry. As for example, in the Moebius strip with twisted strip geometry motion of the electrons along the transverse direction has an important contribution on persistent current. Due to the peculiar topology of the Moebius strip it cannot be compressed into a one-dimensional structure unlike a regular multi-channel cylindrical ring, and it is expected that the persistent currents may exhibit flux-periodicities other than the elementary flux-quantum period ($\phi_0 = ch/e$). In this article, we have studied in detail the magnetic response of the rings with Moebius strip geometry and its dependence on the transverse hopping.

This dissertation is organized as follow. In the introductory chapter, we briefly describe some extraordinary mesoscopic phenomena. In chapter 2, we study the phenomenon of persistent current in the ordered and disordered rings within the one-electron picture. The effects of electron-electron interaction on the persistent currents are investigated in chapter 3. In chapter 4, we show that the contributions of the higher order hopping integrals are quite important for the enhancement of persistent currents in the disordered mesoscopic rings. In chapter 5, we examine the behavior of the low-field magnetic response of persistent currents by calculating the magnetic susceptibility in the limit $\phi \to 0$. The topological effect on persistent current and also the sign of the low-field currents in Moebius strips are discussed in chapter 6. Finally, we conclude in chapter 7.

Chapter 1

Introduction

An emerging tendency in modern material science is to propose and investigate systems containing smaller and smaller structures. These smaller structures approach the so-called mesoscopic or nanoscopic regimes in which quantum effects become much more significant for the behavior of these materials. This situates mesoscopic physics at the interface of statistical and quantum pictures. The mesoscopic systems are very much smaller than the large-scale objects and they often have unusual physical and chemical properties. The study of the mesoscopic systems provides a clear understanding of the behavior of a material as it goes from a few atoms to large visible and tangible objects.

1.1   The Mesoscopic Regime

The mesoscopic scale refers to the length scale at which one can reasonably describe the properties of a material or a phenomenon without discussing the behavior of the individual atoms. For solids this is typically a few to ten nanometers and involves averaging over a few thousand atoms or molecules. In this scale the expected fluctuations of the averaged physical quantities due to the motion and behavior of individual particles can be reduced below some desirable threshold (often to a few percent) and it must be rigorously established within the context of any particular problem. In the mesoscopic regime, behavior of a system is considerably influenced by quantum interference of the electronic wave functions. The quantum phase coherence, essential for the appearance of interference effects, is preserved only during a finite time τ_ϕ called

the phase coherence time. In electronic conductors, the finite phase coherence time corresponds to a phase coherence length L_ϕ over which the electrons can travel before their phase coherence gets lost. Mesoscopic quantum effects appear when the typical time or length scales of the system are smaller than the phase coherence time or length, respectively. In many cases this means that the relevant system size L must be smaller than the phase coherence length L_ϕ. For an electron, the phase coherence time/length is limited by electron-electron and electron-phonon scattering. These processes are important at high temperatures, but both are suppressed at low temperatures implying that the phase coherence time/length is strongly material and temperature dependent.

The mesoscopic regime is therefore characterized by small time and/or length scales and low temperatures. When temperature is lowered, the phase coherence time/length increases (by a factor T^{-1}), and the mesoscopic regime gets extended. At sub-Kelvin temperatures, the time and the length scales in semiconductor samples are of the order of picoseconds and micrometers respectively.

1.2   Some Extraordinary Mesoscopic Phenomena

The samples like quantum dots, quantum wires, two-dimensional electron gases in semiconductor heterostructures, etc., exhibit many exotic physical properties. Here we briefly describe some spectacular effects that appear in such systems as a consequence of quantum phase coherence of the electronic wave functions.

1.2.1   Aharonov-Bohm Oscillations

One of the most remarkable consequences of quantum phase coherence is the Aharonov-Bohm (AB) oscillations in the conductance of normal metal mesoscopic rings. At very low temperature superposition of the electronic wave functions for electron propagation along the two arms of the ring becomes important. The pioneering experiment on AB effect was done on a ring-shaped resistor made from a 38 nm film of polycrystalline gold. The diameter of the

ring was 820 nm and the thickness of the wires was 40 nm [1]. The conductance of the ring was observed to oscillate as a function of magnetic flux enclosed by the ring with $h/|e|$ periodicity [2]:

$$g = g_0 + \hat{g} \cos \left[\frac{|e|BS}{\hbar} + \overline{\phi} \right] \tag{1.1}$$

where S is the area enclosed by the ring and B is the magnetic filed perpendicular to the plane of the ring.

1.2.2 Integer Quantum Hall Effect

One of the most spectacular discoveries of 1980s was the integer quantum Hall effect [3] as a result of quantum phase coherence of the electronic wave functions in the two-dimensional electron gas systems. In the Hall measurement, one drives a current along a conductor (two-dimensional electron gas), and measures the longitudinal voltage V_x and the transverse Hall voltage V_H as a function of the magnetic field B applied perpendicular to the plane of the conductor. According to the classical Drude formula, the Hall resistance R_H should be linearly proportional to the field strength B and the longitudinal resistance R_x should remain unaffected by the magnetic field. This behavior holds true only when magnetic field is very weak. In strong magnetic field and at low temperature, one gets completely different behavior which cannot be explained by the classical Drude model. In high field longitudinal resistance shows oscillatory behavior, while Hall resistance shows step-like behavior with sharp plateaus. The values of R_H on these plateaus are given by h/ne^2, where n is an integer with values $1, 2, 3, \ldots$ and it turns out that these values of R_H are highly reproducible with great precision and are also very robust so that they are often used as the standard of resistance. The integer quantum Hall effect is a purely quantum mechanical phenomenon due to the formation of the Landau levels and many good reviews on IQHE are available in the literature [4, 5, 6].

1.2.3 Fractional Quantum Hall Effect

At extremely high magnetic fields and low temperatures, a two-dimensional electron gas shows additional plateaus in the Hall resistance at fractional filling factors and this phenomenon was discovered in 1982 [7]. Unlike the integer quantum Hall effect, it has been observed that the Coulomb correlation between the electrons becomes important for the interpretation of the fractional quantum Hall effect and the presence of fractional filling has been traced back to the existence of correlated collective quasi-particle excitations [8]. An extensive review on this topic can be found in [5].

1.2.4 Conductance Fluctuations and Quantization

In the mesoscopic regime, conductance of disordered wires exhibits pronounced fluctuations as a function of external parameters, like the magnetic field or the Fermi energy. These fluctuations were observed [9] only at very low-temperature which are perfectly reproducible and represent a fingerprint of the quantum effects in the sample. The fluctuations appear due to the interference of electronic wave functions corresponding to different pathways that the electrons can take when traversing through the system. The most important feature of this conductance fluctuations is that their typical amplitude is universal in the diffusive regime [10]. The fluctuations are always of the order of the conductance quantum e^2/h and depend only on the basic symmetries of the system [11].

The conductance of ballistic quantum point contacts was found [12, 13] to be quantized in units of $2e^2/h$ and a recent experiment [14] demonstrates that the conductance quantization can be observed even in an extremely simple setup. A quantum point contact is a very narrow link between two conducting materials formed by imposing a narrow constriction into them. With the decrease of the width (W) of constriction it has been observed that conductance goes down in quantized steps. This is due to the fact that although the width of the constriction changes continuously, the number of sub-bands or transverse modes (M) changes in discrete steps. This discreteness is not evident if the constriction is several thousands of wavelengths wide, since then a very

small fractional change in W changes M by many integers.

1.2.5 Persistent Currents

The physics of small metallic rings provides an excellent testing ground for many ideas of basic physics. In thermodynamic equilibrium, a small metallic ring threaded by magnetic flux ϕ supports a current that does not decay dissipatively even at non-zero temperature. It is the well-known phenomenon of persistent current in mesoscopic normal metal rings. This is a purely quantum mechanical effect and gives an obvious demonstration of the Aharonov-Bohm effect [15]. The possibility of persistent current was predicted in the very early days of quantum mechanics by Hund [16], but their experimental evidences came much later only after realization of the mesoscopic systems. In 1983, Büttiker *et al.* [17] predicted that persistent current can exist in the mesoscopic normal metal rings threaded by magnetic flux even in the presence of impurity. In a pioneering experiment Levy *et al.* [18] first gave the experimental evidence of persistent current in the mesoscopic normal metal rings and later the existence of the persistent current was further confirmed by several experiments [19, 20, 21, 22]. However, the experimental results do not agree with the theoretical predictions. The measured amplitudes of the currents are orders of magnitude larger than the theoretical estimates, both half-integer and integer flux-quantum ($\phi_0 = ch/e$) periodicities are observed, and, the low-field magnetic susceptibility are found to be diamagnetic as well as paramagnetic. Normal metals are intrinsically disordered and electron-electron interaction becomes important as the electrons are not screened much at the mesoscopic length scale. To grasp the experimental behaviors of the persistent current one has to focus attention on the interplay of quantum phase coherence, electron-electron correlation and disorder. This is a highly complex problem that has been addressed quite extensively over the last twenty years both theoretically [23, 24, 25, 26, 27, 28, 29, 30, 31, 32, 33, 34, 35, 36, 37, 38, 39] as well as experimentally [18, 19, 20, 21, 22]. A detailed discussion about the phenomenon of the persistent current in mesoscopic normal metal loops will be available in the forthcoming chapters of this article. For the sake of simplicity, throughout our studies we use the units $c = e = h = 1$.

Chapter 2

Persistent Current in Non-Interacting Single-Channel and Multi-Channel Mesoscopic Rings

Our aim of this chapter is to study persistent currents in some small non-superconducting loops threaded by a magnetic flux ϕ. A conducting ring, penetrated by a magnetic flux ϕ, carries an equilibrium current in its ground state that *persists* (does not decay) in time. An electrically charged particle moving around the ring but not entering the region of magnetic flux, feels no (classical) force during its motion. However, the magnetic vector potential $\vec{A}$, related to the magnetic field through the relation $\vec{B} = \vec{\nabla} \times \vec{A}$, affects the quantum state of the particle by changing the phase of its wave function. As a consequence, both thermodynamic and kinetic properties oscillate with the magnetic flux ϕ. Here we present some analytical as well as numerical calculations and study the behavior of persistent current I in mesoscopic rings as a function of flux ϕ, system size L, total number of electrons N_e, chemical potential μ and the strength of disorder W.

2.1 Origin of Persistent Current

In this section we describe how persistent current appears in a small normal metal ring threaded by a magnetic flux ϕ. The schematic representation of the

system is given in Fig. 2.1. The electric field $\mathcal{E}$ associated with the magnetic field B in the ring can be expressed through the relation (Faraday's law)

$$\vec{\nabla} \times \vec{\mathcal{E}} = -\frac{1}{c}\frac{\partial \vec{B}}{\partial t} \tag{2.1}$$

Using the above relation we can determine the electric field $\mathcal{E}$ from the following expressions:

$$\oint_S (\vec{\nabla} \times \vec{\mathcal{E}}).\vec{dS} = -\frac{1}{c}\oint_S \frac{\partial \vec{B}}{\partial t}.\vec{dS} = -\frac{1}{c}\frac{\partial}{\partial t}\oint_S \vec{B}.\vec{dS} = -\frac{1}{c}\frac{\partial \phi}{\partial t} \tag{2.2}$$

where S is the area enclosed by the ring. From the Stoke's theorem we can write,

$$\oint_{loop} \vec{\mathcal{E}}.\vec{dl} = -\frac{1}{c}\frac{\partial \phi}{\partial t} \tag{2.3}$$

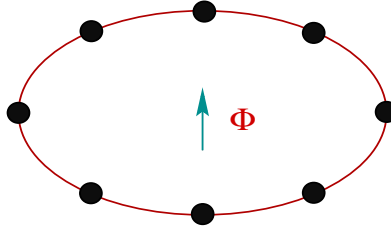and thus the electric field can be written in terms of the time variation of the

Figure 2.1: One-dimensional ring threaded by a magnetic flux ϕ. Filled circles denote the position of the atomic sites. A persistent current I is established in the ring.

magnetic flux ϕ as,

$$\mathcal{E} = -\frac{1}{2\pi rc}\frac{\partial \phi}{\partial t} \tag{2.4}$$

where r is the radius of the ring. Therefore, the force acting on an electron in the ring becomes,

$$F = -\frac{e}{2\pi rc}\frac{\partial \phi}{\partial t} \tag{2.5}$$

and the change in energy or work done for a small displacement $\triangle s$ is,

$$\triangle E = \triangle W = \vec{F}.\vec{\triangle s} = -\frac{e}{2\pi rc}\frac{\triangle \phi}{\triangle t}\triangle s = -\frac{e}{2\pi rc}\triangle \phi \left(\frac{\triangle s}{\triangle t}\right) \tag{2.6}$$

The velocity of the electron in the ring can be expressed as,

$$v = \frac{\triangle s}{\triangle t} = -\frac{2\pi rc}{e}\left(\frac{\triangle E}{\triangle \phi}\right) \tag{2.7}$$

and the persistent current that developed in the ring becomes,

$$I = ef = \frac{ev}{2\pi r} = -c\left(\frac{\triangle E}{\triangle \phi}\right) \tag{2.8}$$

This is the final expression of persistent current and we see that the current can be obtained by taking the first order derivative of the energy eigenvalues with respect to magnetic flux ϕ.

2.2 Non-Interacting One-Channel Rings

This section focuses attention on the behavior of persistent currents in one-channel rings [40] where the currents are computed for the non-interacting electron systems based on the tight-binding formulation. The model Hamiltonian for a N-site ring ($L = Na$, a is the lattice spacing) threaded by a magnetic flux ϕ (in units of the elementary flux quantum $\phi_0 = ch/e$) can be expressed in this form,

$$H = \sum_i \epsilon_i c_i^\dagger c_i + \sum_{<ij>} t\left[e^{i\theta}c_i^\dagger c_j + e^{-i\theta}c_j^\dagger c_i\right] \tag{2.9}$$

where $c_i^\dagger$ (c_i) corresponds to the creation (annihilation) operator of an electron at the site i, t represents the nearest-neighbor hopping strength, ϵ_i's are the on-site energies and $\theta = 2\pi\phi/N$ is the phase factor due to the flux ϕ threaded by the ring. The magnetic flux ϕ enters explicitly into the above Hamiltonian (Eq. 2.9), and the wave functions satisfy the periodic boundary condition which is equivalent to consider the above Hamiltonian at zero flux with the flux-modified boundary conditions:

$$\psi|_{x=L} = exp\left[\frac{2\pi i\phi}{\phi_0}\right]\psi|_{x=0}$$

$$\frac{d\psi}{dx}\bigg|_{x=L} = exp\left[\frac{2\pi i\phi}{\phi_0}\right]\frac{d\psi}{dx}\bigg|_{x=0} \tag{2.10}$$

here x varies between 0 to L and is expressed as $x = L\theta'/2\pi$, where θ' is the azimuthal angle, the spatial degrees of freedom of the electron in the ring.

2.2.1   Impurity Free Rings

In order to reveal the basic properties of persistent currents, let us begin our discussion with the simplest possible system which is the case of impurity free non-interacting electron model.

Energy Spectra

For perfect ring, setting $\epsilon_i = 0$ we get the energy of nth eigenstate as,

$$E_n(\phi) = 2t \cos\left[\frac{2\pi}{N}\left(n + \frac{\phi}{\phi_0}\right)\right] \tag{2.11}$$

where $n = 0, \pm1, \pm2, \ldots$. In Fig. 2.2, we plot the energy-flux (E-ϕ) characteristics for a perfect ring considering the system size $N = 10$. The energy levels of the ring are periodic in ϕ with period ϕ_0. At an integer or half-integer flux
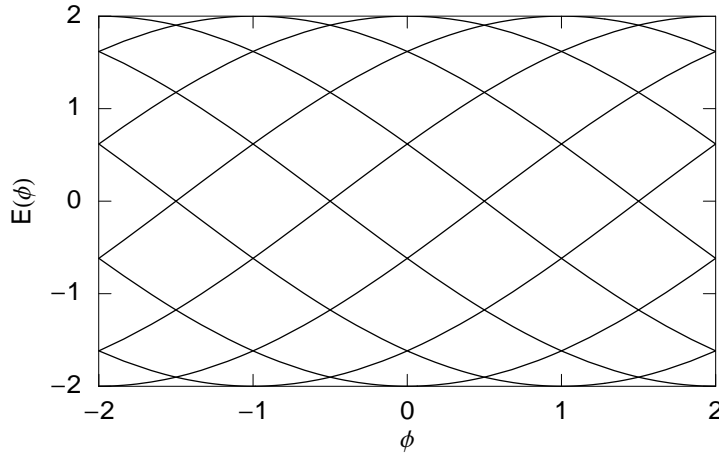

Figure 2.2: Electron energy levels as a function of the magnetic flux ϕ for a one-dimensional impurity-free ring considering the system size $N = 10$.

quantum, the energy levels have a maximum or a minimum, and accordingly, at these values of ϕ current should vanish. Here we discuss the current-flux (I-ϕ) characteristics for the two different cases. In one case we take the rings with fixed number of electrons N_e, and in the other case the rings have some fixed chemical potential μ.

Persistent Current: Rings with Fixed N_e

The current carried by the nth energy eigenstate, whose energy is given by Eq. 2.11, can be obtained through the expression,

$$I_n(\phi) = \left(\frac{4\pi t}{N\phi_0}\right) \sin\left[\frac{2\pi}{N}\left(n + \frac{\phi}{\phi_0}\right)\right] \qquad (2.12)$$

At absolute zero temperature $(T = 0)$, the total persistent current is obtained by taking the sum of individual contributions from the lowest N_e energy eigen-
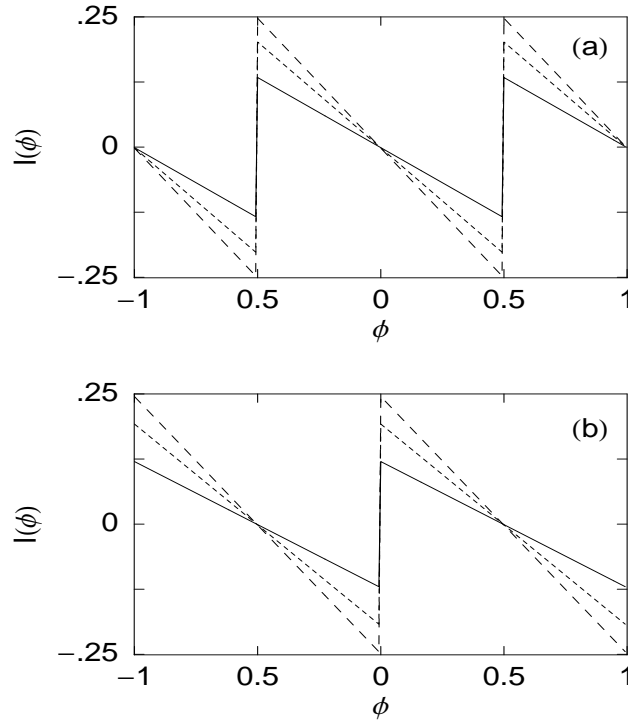

Figure 2.3: Current-flux characteristics for the one-channel perfect rings ($N = 50$) described with fixed number of electrons. The solid, dotted and dashed curves in Fig. 2.3(a) correspond to $N_e = 9$, 15 and 23 electrons respectively, while in Fig. 2.3(b) these curves correspond to $N_e = 8$, 14 and 22 electrons respectively.

states. In Fig. 2.3, we plot the current-flux characteristics for some one-channel perfect rings ($N = 50$) in which Fig. 2.3(a) corresponds to the results for the rings with odd N_e and Fig. 2.3(b) represents the results for the rings with even

N_e. It is observed that the current shows saw-tooth like behavior with sharp transitions at half-integer and integer flux quanta for the rings with odd and even N_e respectively. For all such cases, the current varies periodically with ϕ showing ϕ_0 periodicity.

Persistent Current: Rings with Fixed μ

For the rings described with fixed chemical potential μ, instead of N_e, the total persistent current at $T = 0$ will be obtained by adding all individual contributions from the energy levels with energies less than or equal to μ. As
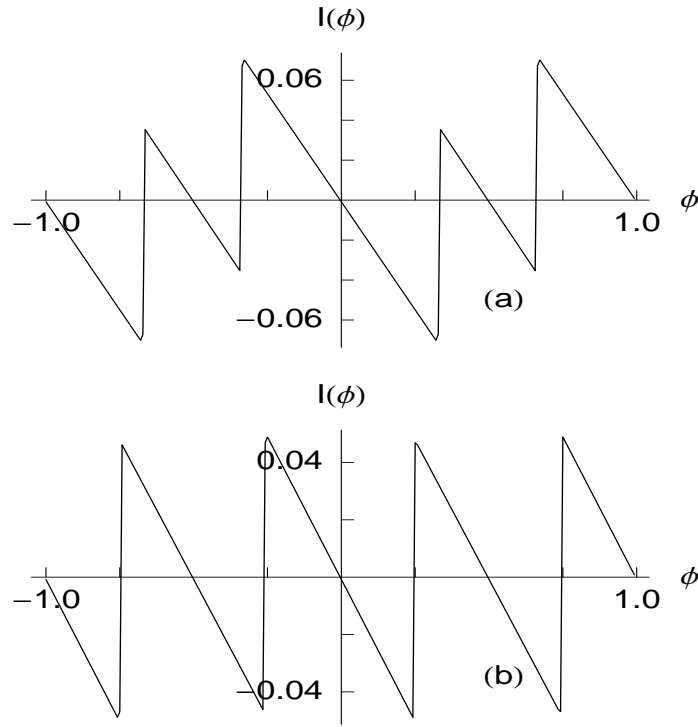
Figure 2.4: Current-flux characteristics for the one-channel perfect rings ($N = 100$) described with constant μ, where (a) $\mu = -1$ and (b) $\mu = -1.25$.

the chemical potential is fixed, the total number of electrons varies as a function of the magnetic flux ϕ except for some special choices of μ, where the rings contain fixed number of electrons. In Fig. 2.4, we plot the persistent currents for some one-channel perfect rings those are described with fixed chemical

potential μ. Here we take the ring size $N = 100$. Fig. 2.4(a) and Fig. 2.4(b) correspond to the persistent currents for the rings with $\mu = -1$ and -1.5 respectively. Our results predict that several additional kink-like structures appear at different field points and their positions also depend on the choices of μ. For all these cases the current gets only ϕ_0 periodicity.

2.2.2 Rings with Impurity

Metals are intrinsically disordered which tends to decrease persistent current due to the localization effect [41] of energy eigenstates. In order to emphasize the role of impurities on persistent currents now we concentrate our study on the rings in the presence of disorder.

Energy Spectra

In the presence of impurity in the ring, gaps open at the points of intersection of the energy levels, in the same way as band gaps form in the band-structure
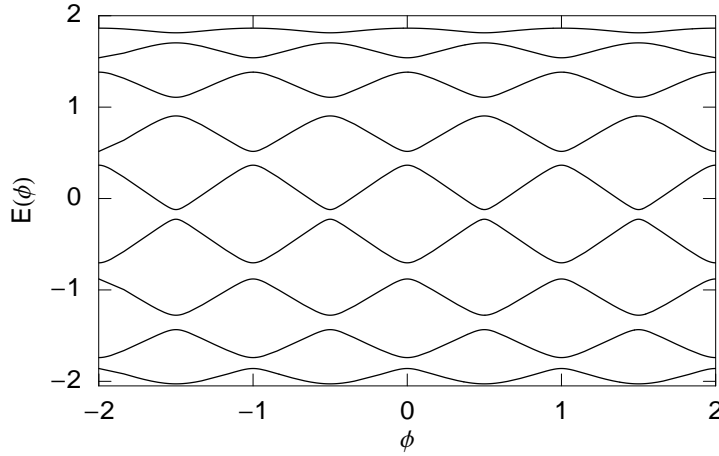
Figure 2.5: Electron energy levels as a function of the flux ϕ for a one-channel ring ($N = 10$) in the presence of impurity with strength $W = 1$.

problem, and they vary continuously with the magnetic flux ϕ. Fig. 2.5 shows the electron energy levels as a function of the flux ϕ for a one-channel ring ($N = 10$) in the presence of diagonal disorder. To introduce the impurities in the ring, we choose the site energies ϵ_i's randomly from a "Box" distribution

function of width $W = 1$. This continuous variation of the energy levels with flux ϕ is due to the removal of the degeneracies of the energy eigenstates in the presence of impurity in the ring.

Persistent Current: Rings with Fixed N_e

In Fig. 2.6, we plot the persistent currents for some one-channel disordered rings considering the ring size $N = 50$ and the impurity strength $W = 1$. Fig. 2.6(a) corresponds to the persistent currents for the rings described with
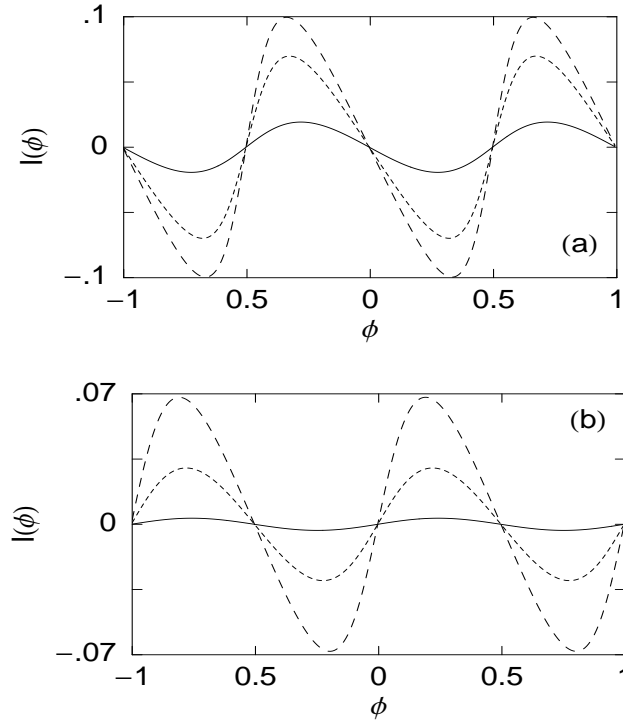
Figure 2.6: I-ϕ characteristics for the disordered ($W = 1$) one-channel rings ($N = 50$) with fixed number of electrons. The solid, dotted and dashed curves in Fig. 2.6(a) correspond to $N_e = 9$, 15 and 23 electrons respectively, while in Fig. 2.6(b) they correspond to $N_e = 8$, 14 and 22 electrons respectively.

odd number of electrons, while Fig. 2.6(b) represents the currents for the rings with even number of electrons. It is observed that the current varies continuously as a function of ϕ and gets much reduced amplitude compared to the results obtained in the impurity-free rings (see Fig. 2.3). The continuous vari-

ation of the current is clearly visible from the variation of the energy spectra since they become continuous as long as the impurities are introduced in the ring. On the other hand, the suppression of the current amplitudes is due to the localization effect of the energy eigenstates in the presence of impurity. Here all the results are described for some typical disordered configurations of the ring, and in fact we examine that the qualitative behavior of the persistent currents do not depend on the specific realization of the disordered configurations. This is the generic feature of persistent current for any one-channel non-interacting rings in the presence of impurity those are described with fixed number of electrons N_e.

Persistent Current: Rings with Fixed μ

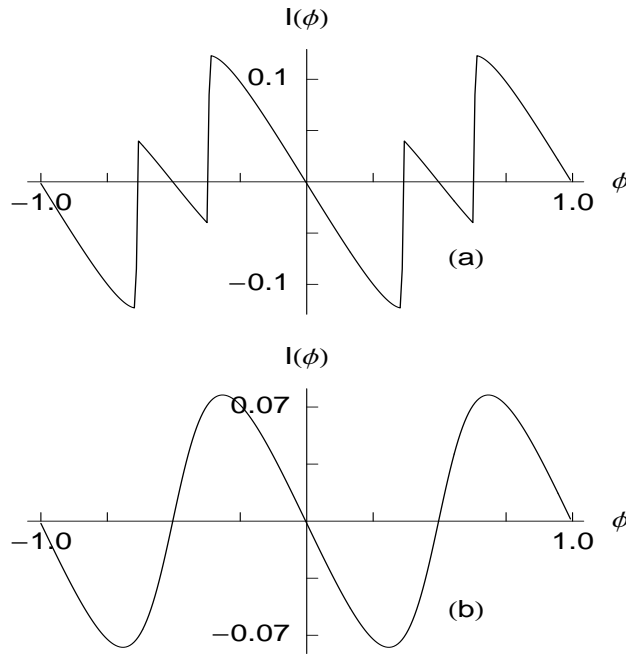The behavior of the current-flux characteristics is quite interesting in the pres-

Figure 2.7: I-ϕ characteristics for the disordered ($W = 1$) one-channel rings ($N = 50$) described with constant μ, where (a) $\mu = -1$ and (b) $\mu = -1.25$.

ence of impurity for the rings described with fixed chemical potential μ, instead of N_e. As representative example, in Fig. 2.7 we plot the I-ϕ characteristics

for some one-channel disordered rings those are described with fixed μ, where Fig. 2.7(a) represents the result for the ring with $\mu = -1$ and Fig. 2.7(b) denotes the result for the ring considering $\mu = -1.5$. From these results we can emphasize that depending on the choices of μ the current shows different behavior as a function of ϕ and in all such cases the current exhibits only ϕ_0 periodicity.

2.3   Non-Interacting Multi-Channel Systems

Now we focus our study on the behavior of persistent currents in non-interacting multi-channel systems [40]. A schematic representation of such a multi-channel system of cylindrical geometry threaded by a magnetic flux ϕ is given in Fig. 2.8. Considering the lattice spacing both in the longitudinal and trans-
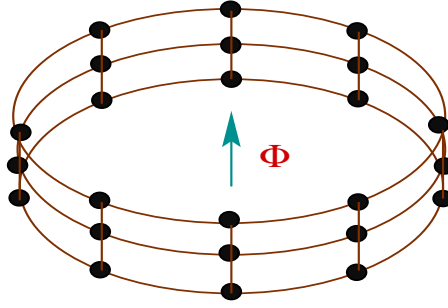

Figure 2.8: Schematic view of a multi-channel cylinder threaded by a magnetic flux ϕ.

verse directions are identical i.e., the surface of the cylinder forms a square lattice, we can write the Hamiltonian of the system by the tight-binding formulation as,

$$H = \sum_x \epsilon_x c_x^\dagger c_x + \sum_{<xx'>} \left[t_{xx'} e^{i\theta_{xx'}} c_x^\dagger c_{x'} + t_{xx'} e^{-i\theta_{xx'}} c_{x'}^\dagger c_x \right] \qquad (2.13)$$

where ϵ_x is the site energy of the lattice point x of coordinate, say, (i, j). $t_{xx'}$ is the hopping strength between the lattice points x and x' and $\theta_{xx'}$ is the phase factor acquired by the electron due to the longitudinal hopping in the presence of magnetic flux ϕ. The study of persistent currents in such multi-channel systems becomes much more relevant compared to strictly one-dimensional

rings (see Fig. 2.1), where we get only one channel that carries current, since most of the conventional experiments are performed in rings with finite width. Here we will describe the characteristic properties of persistent currents for some non-interacting multi-channel rings concerning the dependence of the current on total number of electrons N_e, chemical potential μ, strength of disorder W and number of channels. All the results studied here are performed only at absolute zero temperature $(T = 0)$.

2.3.1 Energy Spectra

In order to present the behavior of persistent currents in mesoscopic multi-channel systems, let us first describe the energy-flux characteristics of a small cylindrical system that threads a magnetic flux ϕ. To have a deeper insight to the problem we begin our discussion with the simplest possible system which can be calculated analytically. This is the case of a two-layer impurity free cylinder threaded by a magnetic flux ϕ. This cylindrical system can be treated as two one-channel rings placed one above the other and they are connected by some vertical bonds (like as in Fig. 2.8). For strictly one-dimensional ring i.e., for one layer the energy of nth eigenstate is expressed in the form $E_n(\phi) = 2t \cos \left[\frac{2\pi}{N} \left(n + \frac{\phi}{\phi_0} \right) \right]$ (see Eq. 2.11), where $n = 0, \pm1, \pm2, \ldots$. Here t is the nearest-neighbor hopping strength and N is the total number of lattice points in the ring. The behavior of such energy levels as a function of flux ϕ is shown in Fig. 2.9(a), where we take $N = 10$. From this figure it is observed that the energy levels are bounded within the range -2 to 2 in the scale of t and the crossing of the energy levels (flux points where the energy levels have degeneracy) occurs at half-integer or integer multiples of ϕ_0. Now as we add another one ring with the previous one-dimensional ring and connect it by N vertical bonds it becomes a cylinder with two layers. For such a system, we get two different energy bands of discrete energy levels, each of which contains N number of energy levels and they are respectively expressed in the form, $E_{1n}(\phi) = -t + 2t \cos \left[\frac{2\pi}{N} \left(n + \frac{\phi}{\phi_0} \right) \right]$ and $E_{2n}(\phi) = -t + 2t \cos \left[\frac{2\pi}{N} \left(n + \frac{\phi}{\phi_0} \right) \right]$, where the symbol n corresponds to the same meaning as above and t is the nearest-neighbor hopping strength which is identical both for the longitudinal and transverse directions. In Fig. 2.9(b), we plot the energy levels of a small

impurity-free cylinder considering $N = 10$, where the solid and the dotted curves correspond to the energy levels in the two separate energy bands respectively. These two different energy bands are bounded respectively in the
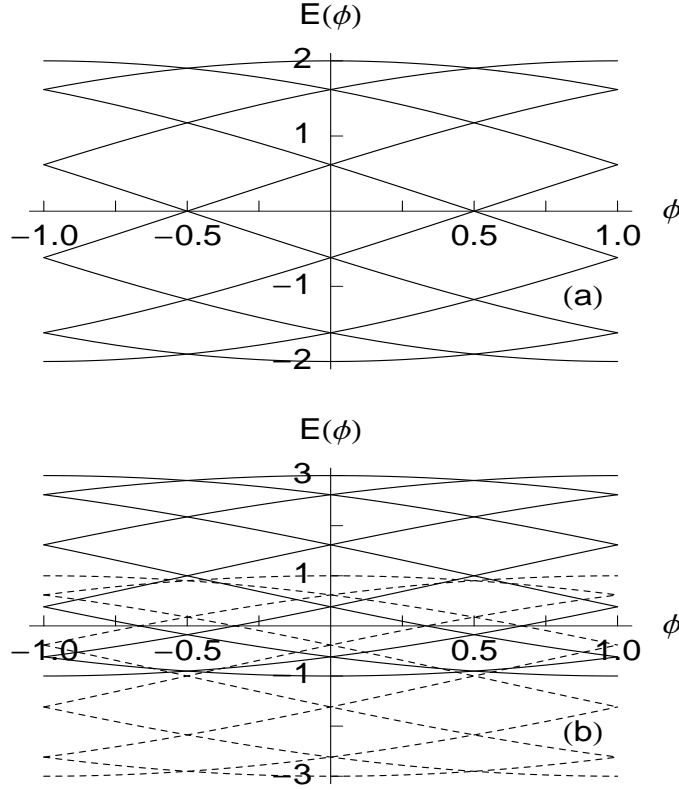

Figure 2.9: Energy levels as a function of the magnetic flux ϕ, for (a) the perfect ring (one layer) with $N = 10$ and (b) the perfect cylinder with two layers taking $N = 10$ in each of these layers.

range -1 to 3 and -3 to 1 in the scale of t. Accordingly, an overlap energy region appears for the two energy bands in the range -1 to 1 as shown in the figure (Fig. 2.9(b)). In this overlap region, the energy levels cross each other at several other flux points in addition to the half-integer and integer multiples of ϕ_0 which provide different characteristic features of persistent currents. For cylinders with more than two layers, we get more energy bands like above and therefore several other overlap energy regions appear in energy spectra.

In the presence of impurity in multi-channel cylinders, gaps open at the

crossing points of the energy levels and they become a continuous function of the flux ϕ, like as in the one-channel disordered rings (Fig. 2.5). In all such perfect and disordered multi-channel cylinders, energy levels vary periodically with period ϕ_0.

Now we will investigate the characteristic features of persistent currents for some small cylindrical systems and our results might be quite helpful to explain the characteristic properties of persistent currents for larger system sizes.

2.3.2   Persistent Current

Perfect Cylinders

In this section we study persistent currents of some impurity-free multi-channel systems of cylindrical geometry with two layers concerning the dependence of the current on total number of electrons N_e and chemical potential μ. As illustrative example, in Fig. 2.10 we plot the current-flux characteristics of some perfect cylinders considering $N = 100$ in each of these two layers. Let us first describe the behavior of persistent currents for the cylinders those are described with fixed number of electrons. The first column of Fig. 2.10 corresponds to the currents for the systems with fixed N_e. To emphasize the effect of the energy overlap region on persistent currents here we study the systems for three different values of N_e. Fig. 2.10(a) and Fig. 2.10(c) correspond to the currents for the systems with $N_e = 25$ (low) and $N_e = 185$ (high) respectively. The result for the intermediate value of N_e ($N_e = 100$) is shown in Fig. 2.10(b). It is shown that both for the low and the high values of N_e, the persistent currents get saw-tooth like nature with sharp transitions only at half-integer multiple of ϕ_0, similar to that of strictly one-channel impurity-free rings with odd N_e (see Fig. 2.3(a)). This behavior can be explained as follows. For the system with $N_e = 25$, the net persistent current is obtained by taking the sum of the lowest 25 energy eigenstates those lie below the energy overlap region. Now away from this overlap region, the energy levels behave exactly in the same way with strictly one-channel rings and therefore the current shows similar kind of saw-tooth shape as observed in one-channel

rings. On the other hand, for the system with $N_e = 185$ the situation is quite different than the previous one. To obtain the net current for this case we cross the overlap energy region since the highest energy level that contributes current lies far above of this overlap region. The net contribution to the current
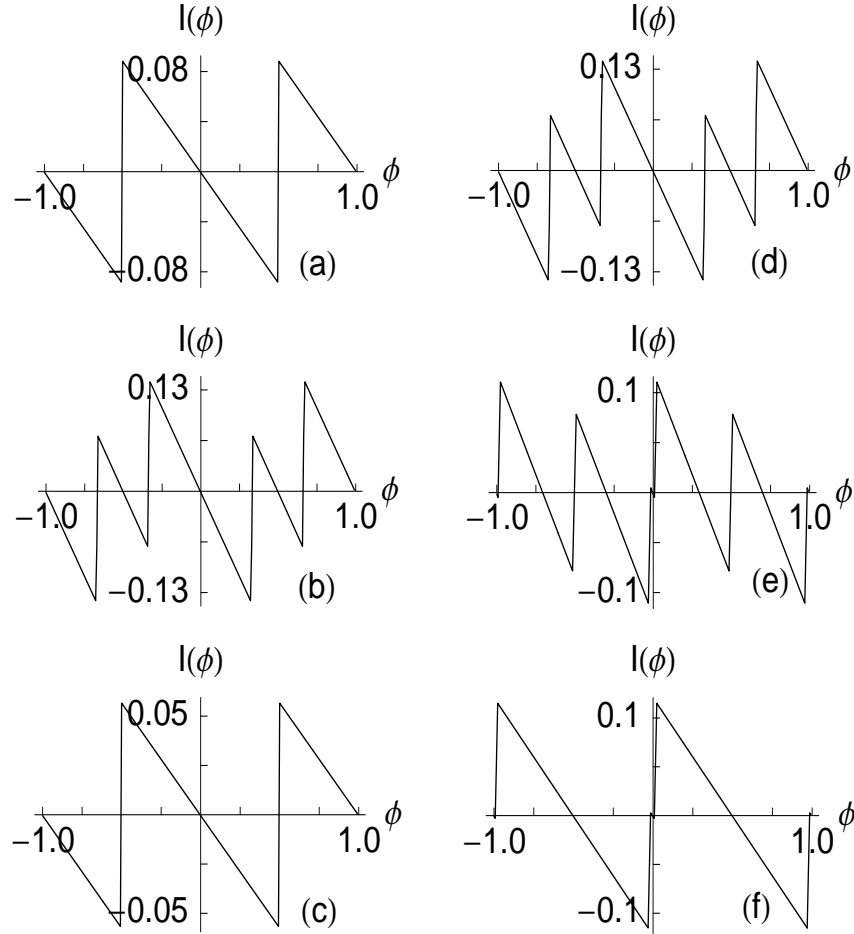
Figure 2.10: I versus ϕ curves of the perfect cylinders with two layers taking $N = 100$ in each layer. The results for the fixed N_e are plotted in the first column, where (a) $N_e = 25$, (b) $N_e = 100$ and (c) $N_e = 185$, while in the second column the results are plotted for the fixed μ, where (d) $\mu = 0$, (e) $\mu = -0.5$ and (f) $\mu = -1.5$.

from the energy levels within this overlap region vanishes and therefore no new feature appears in the persistent current compared to the system with $N_e = 25$. Now we describe the result plotted in Fig. 2.10(b), where the system

contains intermediate value of N_e ($N_e = 100$). For such a case the persistent current shows some additional kink-like structures across $\phi = \pm 0.5$. These kinks are due to the different contributions of the energy levels in the overlap energy region, since in the overlap region energy levels have more degeneracy at several other flux points rather than the half-integer and integer multiples of ϕ_0. For other multi-channel systems with more than two layers, some more kinks may appear in persistent current at different values of ϕ depending on the choice of N_e and the number of layers.

In multi-channel systems where we fix the chemical potential μ instead of the total number of electrons N_e, we also get different kink-like structures in the persistent currents as observed from the results plotted in the second column of Fig. 2.10. For all such systems described either with fixed N_e or μ, the current exhibits only ϕ_0 flux-quantum periodicity.

Dirty Cylinders

To illustrate the effect of the impurity on persistent currents in multi-channel systems, here we concentrate our study in some dirty cylinders considering the same system size as taken above for the perfect systems. In Fig. 2.11, we plot the current-flux characteristics for some disordered cylinders where the impurities are given only in the site energies (ϵ_x) by choosing them randomly from a "Box" distribution function of width $W = 1$. All the results are plotted for isolated disordered configurations of the system. The first column of Fig. 2.11 represents the persistent currents for the cylinders described with fixed N_e, while the second column of this figure corresponds to the currents for the systems with fixed μ. It is observed that, in all these cases the persistent current varies continuously as a function of flux ϕ showing ϕ_0 periodicity. The explanation of such a continuous variation has already been described in our previous studies. Another significant point observed from Fig. 2.11(a) and Fig. 2.11(b) is that, the slope of the current in the zero-field limit ($\phi \to 0$) changes in opposite direction though both for the two cases the systems contain even number of electrons. This provides the signature of random sign of low-field currents in multi-channel systems. The detailed description of low-field magnetic response will be available in chapter 5.
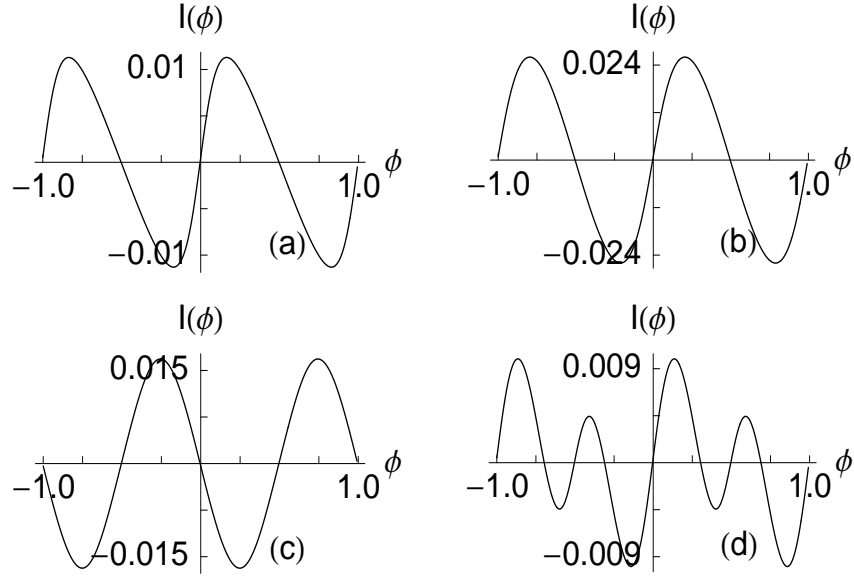
Figure 2.11: Current-flux characteristics for the disordered ($W = 1$) cylinders with two layers taking $N = 100$ in each layer. The results for the fixed N_e are plotted in the first column, where (a) $N_e = 50$ and (b) $N_e = 100$, while the results for the constant μ are plotted in the second column, where (c) $\mu = 0$ and (d) $\mu = -0.5$.

Thus we can emphasize that the behavior of persistent current in multi-channel systems strongly depends on the disordered configurations, total number of electrons N_e, chemical potential μ and also on the total number of channels.

Chapter 3

Effect of Electron-Electron Correlation on Persistent Current in One-Channel Rings

The phenomenon of persistent current in small conducting ring threaded by a magnetic flux ϕ was predicted in the pioneering work of Büttiker, Imry and Landauer [17], and since then it has been discussed in several theoretical papers [23, 24, 25, 26, 27, 28, 29, 30, 31, 32, 33, 34]. Although this phenomenon is thought to be qualitatively understood within the framework of one-electron picture [17, 24, 25, 26, 27, 28, 29, 30, 31, 32], but it fails to explain many experimental results [18, 19, 20, 21, 22]. A typical example of such discrepancy between theory and experiment is that the amplitudes of measured persistent currents are orders of magnitude larger than theoretical predictions. It is generally believed that electron-electron correlation and disorder have major role on the enhancement of persistent currents, but no consensus has yet been reached. Another important controversial issue is that, experimentally both ϕ_0 and $\phi_0/2$ periodicities have been observed and it is also found that the $\phi_0/2$ oscillations near zero magnetic flux exhibit diamagnetic response. The explanation of these results in terms of the ensemble averaged persistent currents is also quite intriguing, and the calculations show that the disordered averaged current crucially depends on the choice of the ensemble [24, 29]. The explanation of experimental results become even much more illusive since recently Kravtsov *et al.* [42] have shown that additional currents may be generated in

rings by other mechanisms which are not experimentally distinguishable from the persistent current.

3.1 Impurity Free Rings

To emphasize the precise role of electron-electron correlation, in this section we focus on the exact calculation of persistent current and Drude weight in perfect one-dimensional Hubbard rings [43] threaded by a magnetic flux ϕ. Our study reveals that, certain aspects of the many-body effects on persistent current have not been investigated in the literature clearly, and here we will show that the Hubbard correlation leads to many significant effects. We restrict ourselves to small Hubbard rings and these results might also be helpful to understand the physical properties of TTF-TCMQ conductors, various aromatic molecules and systems of connected quantum dots[44]. With the new advancements of the nanoscience and technology, it is now possible quite simply to fabricate such small rings, and in a recent experiment Keyser *et al.* [45] reported the evidence of anomalous Aharonov-Bohm oscillations from the transport measurements on small quantum rings with less than ten electrons. The electron-electron interaction becomes much more important in these small rings with very few number of electrons since the Coulomb potential is not screened much, and we will show that the electron-electron interaction provides similar anomalous oscillations in persistent current as a function of magnetic flux ϕ.

We use the Hubbard model to represent the system which for a N-site ring enclosing a magnetic flux ϕ can be written in this form,

$$H = t \sum_\sigma \sum_{i=1}^{N} \left[e^{i\theta} c^\dagger_{i,\sigma} c_{i+1,\sigma} + e^{-i\theta} c^\dagger_{i+1,\sigma} c_{i,\sigma} \right] + U \sum_{i=1}^{N} n_{i\uparrow} n_{i\downarrow} \qquad (3.1)$$

where $c^\dagger_{i\sigma}$ ($c_{i\sigma}$) is the creation (annihilation) operator and $n_{i\sigma}$ is the number operator for the electron in the Wannier state $|i\sigma>$. The parameters t and U are the nearest-neighbor hopping integral and the strength of the Hubbard correlation, respectively. The phase factor $\theta = 2\pi\phi/N$ appears due to the flux ϕ threaded by the ring. Here we set $t = -1$ and use the units $c = e = h = 1$.

3.1.1 Persistent Current

At absolute zero temperature $(T = 0)$, the persistent current in the ring threaded by a magnetic flux ϕ is obtained through the expression [25],

$$I(\phi) = -\frac{\partial E_0(\phi)}{\partial \phi} \tag{3.2}$$

where $E_0(\phi)$ is the ground state energy. We determine this quantity exactly to understand unambiguously the role of the electron-electron interaction on persistent current, and this is obtained by exact numerical diagonalization of the many-body Hamiltonian (Eq. 3.1).

Rings with Two Opposite Spin Electrons

To have a deeper insight to the problem, we first consider two electron systems and begin our study with the simplest possible system which can be treated analytically up to certain level. This is the case of a three-site ring with two opposite spin $(\uparrow, \downarrow)$ electrons. The total Hamiltonian of this system becomes a (9×9) matrix which can be block diagonalized to two sub-matrices by proper choice of the basis states. The orders of the two sub-matrices are (6×6) and (3×3), respectively. This can be achieved by constructing the basis states for each sub-space with a particular value of the total spin S. The basis set $(\mathcal{A})$ for the six-dimensional sub-space, spanned for $S = 0$, is chosen as:

$$\mathcal{A} \equiv \left\{ \begin{array}{l} |\uparrow\downarrow, 0, 0 > \\ |0, \uparrow\downarrow, 0 > \\ |0, 0, \uparrow\downarrow> \\ \frac{1}{\sqrt{2}} (|\uparrow, \downarrow, 0 > - |\downarrow, \uparrow, 0 >) \\ \frac{1}{\sqrt{2}} (|0, \uparrow, \downarrow> - |0, \downarrow, \uparrow>) \\ \frac{1}{\sqrt{2}} (|\downarrow, 0, \uparrow> - |\uparrow, 0, \downarrow>) \end{array} \right\} \quad S = 0$$

On the other hand, the other basis set $(\mathcal{B})$ for the three-dimensional sub-space, spanned for $S = 1$, is chosen as:

$$\mathcal{B} \equiv \left\{ \begin{array}{l} \frac{1}{\sqrt{2}} (|\uparrow, \downarrow, 0 > + |\downarrow, \uparrow, 0 >) \\ \frac{1}{\sqrt{2}} (|0, \uparrow, \downarrow> + |0, \downarrow, \uparrow>) \\ \frac{1}{\sqrt{2}} (|\uparrow, 0, \downarrow> + |\downarrow, 0, \uparrow>) \end{array} \right\} \quad S = 1$$

Table 3.1: Eigenvalues (λ) and eigenstates of two opposite spin electrons for N=3.

Total spin S	λ	Degeneracy	Eigenstate
		$U = 0$	
	-4	1	$\left(-\frac{1}{\sqrt{2}}, -\frac{1}{\sqrt{2}}, -\frac{1}{\sqrt{2}}, -1, -1, 1\right)$
	-1	2	$\left(0, \sqrt{2}, -\sqrt{2}, 1, 0, 1\right)$
			$\left(-\sqrt{2}, 0, \sqrt{2}, -1, 1, 0\right)$
0	2	3	$\left(\frac{1}{\sqrt{2}}, 0, \frac{1}{\sqrt{2}}, 0, 0, 1\right)$
			$\left(0, -\frac{1}{\sqrt{2}}, -\frac{1}{\sqrt{2}}, 0, 1, 0\right)$
			$\left(-\frac{1}{\sqrt{2}}, -\frac{1}{\sqrt{2}}, 0, 1, 0, 0\right)$
	-1	2	$(1, 0, 1)$
1			$(-1, 1, 0)$
	2	1	$(-1, -1, 1)$
Total spin S	λ	Degeneracy	Eigenstate
		$U = 2$	
	$-2\sqrt{3}$	1	$(a, a, a, -1, -1, 1)$
	0	2	$\left(0, \frac{1}{\sqrt{2}}, -\frac{1}{\sqrt{2}}, 1, 0, 1\right)$
			$\left(-\frac{1}{\sqrt{2}}, 0, \frac{1}{\sqrt{2}}, -1, 1, 0\right)$
0	3	2	$\left(0, -\sqrt{2}, \sqrt{2}, 1, 0, 1\right)$
			$\left(\sqrt{2}, 0, -\sqrt{2}, -1, 1, 0\right)$
	$2\sqrt{3}$	1	$(b, b, b, -1, -1, 1)$
	-1	2	$(1, 0, 1)$
1			$(-1, 1, 0)$
	2	1	$(-1, -1, 1)$

In the absence of any magnetic field, we list the energy eigenvalues, eigenstates, and the degeneracy of the levels of this system in Table 3.1 for $U = 0$ and $U = 2$. In this table we set $a = -\sqrt{2}/\left(1 + \sqrt{3}\right)$ and $b = \sqrt{2}/\left(-1 + \sqrt{3}\right)$. Both for $U = 0$ and $U \neq 0$ cases, the two-fold degeneracy gets lifted in the presence of magnetic flux ϕ. It is apparent from this table that the eigenvalues, eigenstates and also the degeneracy of the energy levels are not affected by the correlation in the three-dimensional sub-space. This is due to the fact that the basis set $\mathcal{B}$ does not involve any doubly occupied state but this is not true in the other sub-space. The insertion of the magnetic flux does not alter the

above structure of the Hamiltonian though it becomes now field dependent.

In Fig. 3.1(a), we plot some of the low-lying energy levels $E(\phi)$'s as a function of the magnetic flux ϕ of this three-site ring in the absence of any
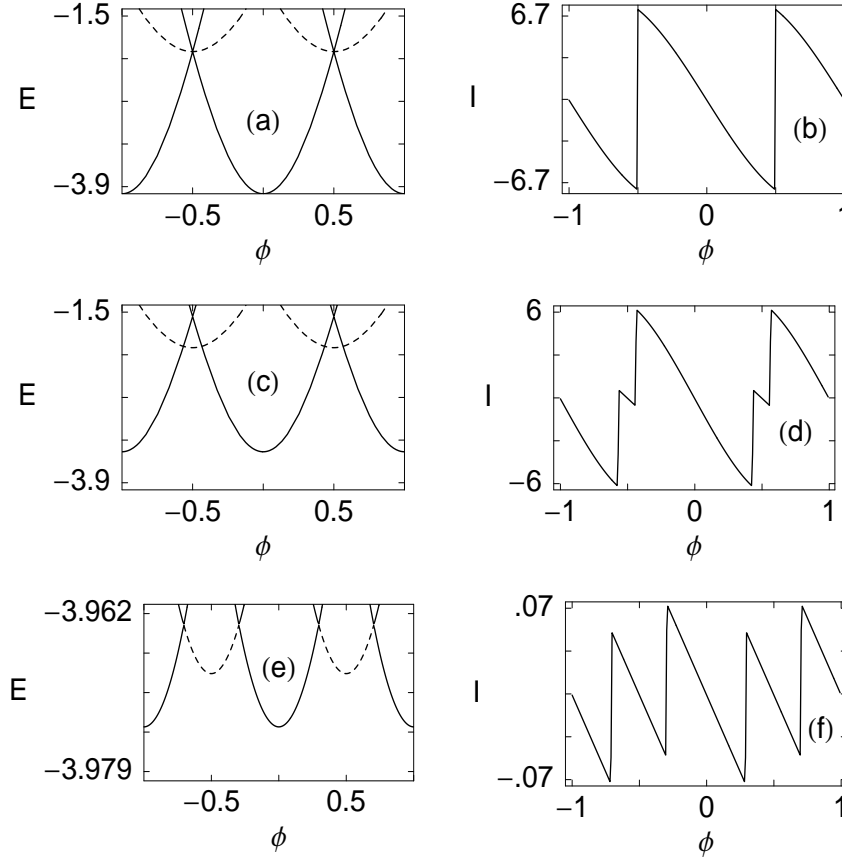

Figure 3.1: The E-ϕ and I-ϕ characteristics of the following two opposite spin $(\uparrow, \downarrow)$ electron systems: (I) $N = 3$, $U = 0$ in (a) & (b); (II) $N = 3$, $U = 2$ in (c) & (d); and (III) $N = 25$, $U = 3$ in (e) & (f).

electron correlation $(U = 0)$, and the corresponding $I(\phi)$ versus ϕ curve is plotted in Fig. 3.1(b). The E-ϕ and I-ϕ curves for $U = 2$ case are given in Fig. 3.1(c) and Fig. 3.1(d) respectively. The dotted curves in Fig. 3.1(a) and Fig. 3.1(c) correspond to the U-independent energy levels as mentioned above. Quite interestingly, from Fig. 3.1(c) we see that even in the presence of interaction, one of the U-independent energy levels becomes the ground state energy level in certain intervals of ϕ (e.g., around $\phi = \pm 0.5$). In other regions of

ϕ, the ground state energy increases due to the correlation and the E_0-ϕ curves become much shallow, as expected. As a result, the usual sawtooth shape of the current-flux characteristics for $U = 0$ changes drastically as plotted in Fig. 3.1(d) and the role of the correlation is quite complex rather than a simple suppression of persistent current as predicted earlier. A sudden change in the direction and the magnitude of the persistent current occurs, solely due to the correlation, around $\phi = \pm 0.5$ and it forms kink-like structures in the current, as illustrated in Fig. 3.1(d). The kinks become wider as we increase the strength of U, and the most significant result is that the persistent current remains invariant inside the kinks irrespective of the correlation strength. It is also seen that, the correlation does not affect the ϕ_0 flux periodicity of the persistent current.

From this above background we can investigate the role of the electron correlation on the persistent current in mesoscopic rings with larger sizes. In Fig. 3.1(e) and Fig. 3.1(f), we display the E-ϕ and I-ϕ characteristics for the ring containing two opposite spin electrons with $N = 25$ and $U = 2$ respectively. These figures respectively resembles Fig. 3.1(c) and Fig. 3.1(d), and it implies that the correlation plays the same role in both the cases. Therefore, we can precisely say that away from the half-filling, a ring consisting of two opposite spin electrons always exhibits kinks in the persistent current for any non-zero value of U.

Rings with Two Up and One Down Spin Electrons

Now we consider rings with two up and one down spin electrons as illustrative examples of three spin electron systems. We plot the E-ϕ and I-ϕ curves for the half-filled ring ($N = 3$ and $n = 3$, where n denotes the number of electrons) with $U = 3$ in Fig. 3.2(a) and Fig. 3.2(b) respectively. We find that the correlation just diminishes the magnitude of the current compared to that of the noninteracting case. In Fig. 3.2(c) and Fig. 3.2(d), we respectively plot the E-ϕ and I-ϕ curves of a non-half-filled ring with $N = 10$ and $U = 3$, while Fig. 3.2(e) and Fig. 3.2(f) are these curves for the $U = 15$ case. The behavior of the persistent current as a function of the flux ϕ are quite different at low and high values of U. From Fig. 3.2(c), it is evident that for the low value

of U all the U-independent energy levels (dotted curves) always lie above the ground state energy of the system, and Fig. 3.2(d) shows that apart from a reduction of the persistent current the I-ϕ curve looks very similar to that of a ring without any interaction. On the other hand, from Fig. 3.2(e) it is
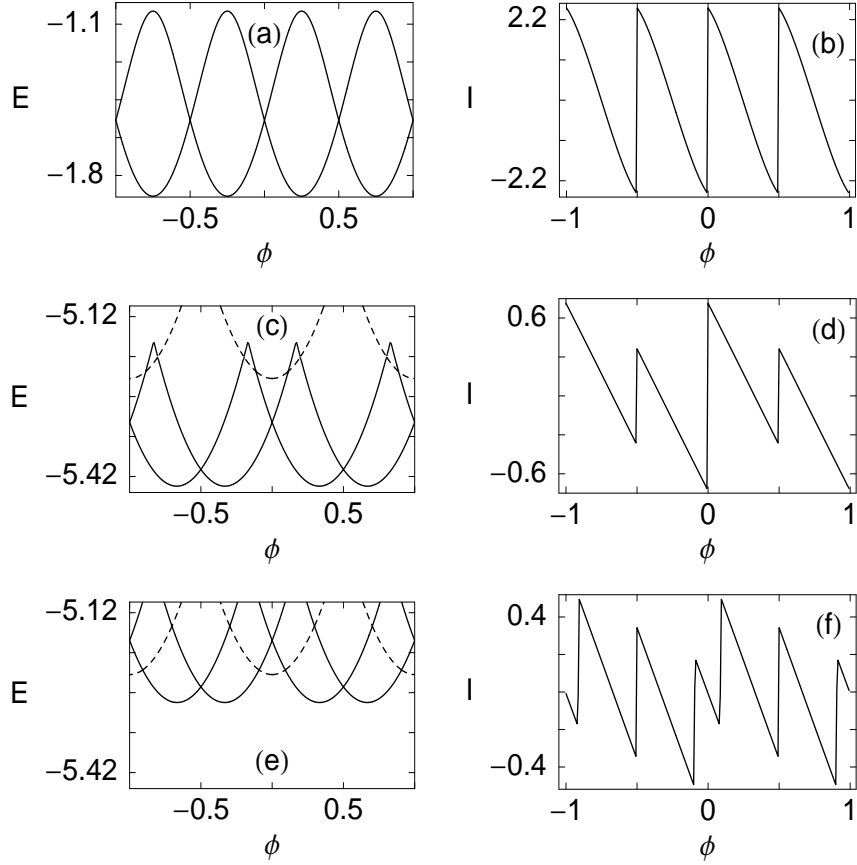

Figure 3.2: The E-ϕ and I-ϕ characteristics of the following three $(\uparrow, \uparrow, \downarrow)$ electron systems: (I) $N = 3$, $U = 3$ in (a) & (b); (II) $N = 10$, $U = 3$ in (c) & (d); and (III) $N = 10$, $U = 15$ in (e) & (f).

observed that for the high value of U one of the U-independent energy levels becomes the ground state energy in certain intervals of ϕ (e.g., around $\phi = 0$) and this produces kinks in the I-ϕ characteristics as depicted in Fig. 3.2(f). Certainly there exists a critical value U_c of the correlation above which the kinks appear in the I-ϕ characteristics. These features of the energy spectra and the persistent currents are the characteristics of any non-half-filled ring

with two up and one down spin interacting electrons. Here we note that the half-filled rings exhibit $\phi_0/2$ periodic currents, while the non-half-filled rings have ϕ_0 periodicity.

Rings with Two Up and Two Down Spin Electrons

Next we consider rings with two up and two down spin electrons as representative examples of four electron system. Let us first describe the half-filled case
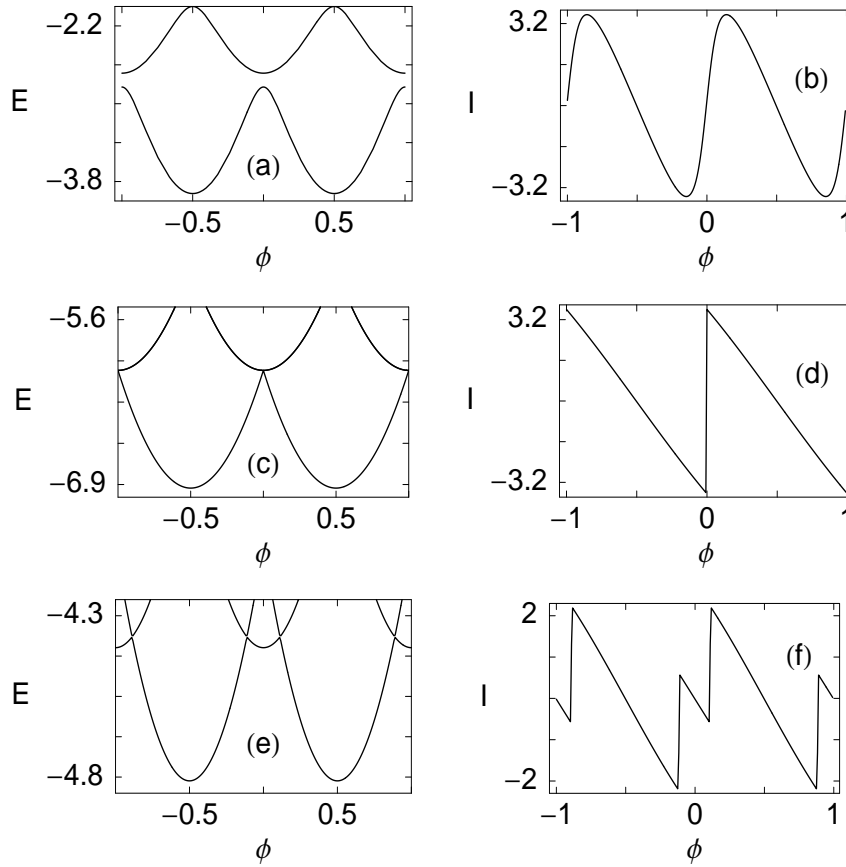

Figure 3.3: The E-ϕ and I-ϕ characteristics of the following four $(\uparrow, \uparrow, \downarrow, \downarrow)$ electron systems: (I) $N = 4$, $U = 2$ in (a) & (b); (II) $N = 6$, $U = 0$ in (c) & (d); and (III) $N = 6$, $U = 6$ in (e) & (f).

($N = 4$ and $n = 4$). In the absence of any electron correlation, sharp discontinuity appears in the persistent current at certain values of ϕ. However, the

effect of the correlation is quite dramatic and it makes the current a continuous function of the flux as plotted in Fig. 3.3(b). This is a quite fascinating result since the correlation drastically changes the analytic behavior of $I(\phi)$, and here we will observe that this result also holds true for the other half-filled systems with even number of electrons. Away from the half-filling we study an interesting typical case of a six-site ring with two up and two down spin electrons. This can be considered as a doubly ionized benzene-like ring, a system with the promise of experimental verification of our predictions. Fig. 3.3(c) and Fig. 3.3(d) show the E-ϕ and I-ϕ characteristics with $U = 0$ respectively, while Fig. 3.3(e) and Fig. 3.3(f) are those plots with $U = 6$. It is observed from Fig. 3.3(f) that the kinks appear in the I-ϕ curve (e.g., around $\phi = 0$) for any non-zero value of U. Here we interestingly note that the kinks are now due to the U-dependent eigenstates. Both the half-filled and non-half-filled rings exhibit ϕ_0 periodic currents.

Rings with Three Up and Two Down Spin Electrons

For specific cases of five electron systems we investigate rings with three up and two down spin electrons. In Fig. 3.4(a) and Fig. 3.4(b), we plot the E-ϕ and I-ϕ curves, respectively for the non-half-filled ring ($N = 5$ and $n = 5$). The magnitude of the current is just diminished due to the electron correlation and we find $\phi_0/2$ periodicity. As a non-half-filled five electron case, here we take a singly ionized benzene-like ring ($N = 6$ and $n = 5$) and determine the persistent current both for low and high values of U. In Fig. 3.4(c) and Fig. 3.4(d), we respectively draw the E-ϕ and I-ϕ curves considering the correlation strength $U = 2$, while these diagrams are plotted in Fig. 3.4(e) and Fig. 3.4(f) with $U = 120$. From Fig. 3.4(d) and Fig. 3.4(f), it is clear that like the three electron rings kinks appear in the persistent current only after a critical value of U. This result emphasizes that the characteristic features of the persistent current in mesoscopic Hubbard rings with odd number of electrons are almost invariant.
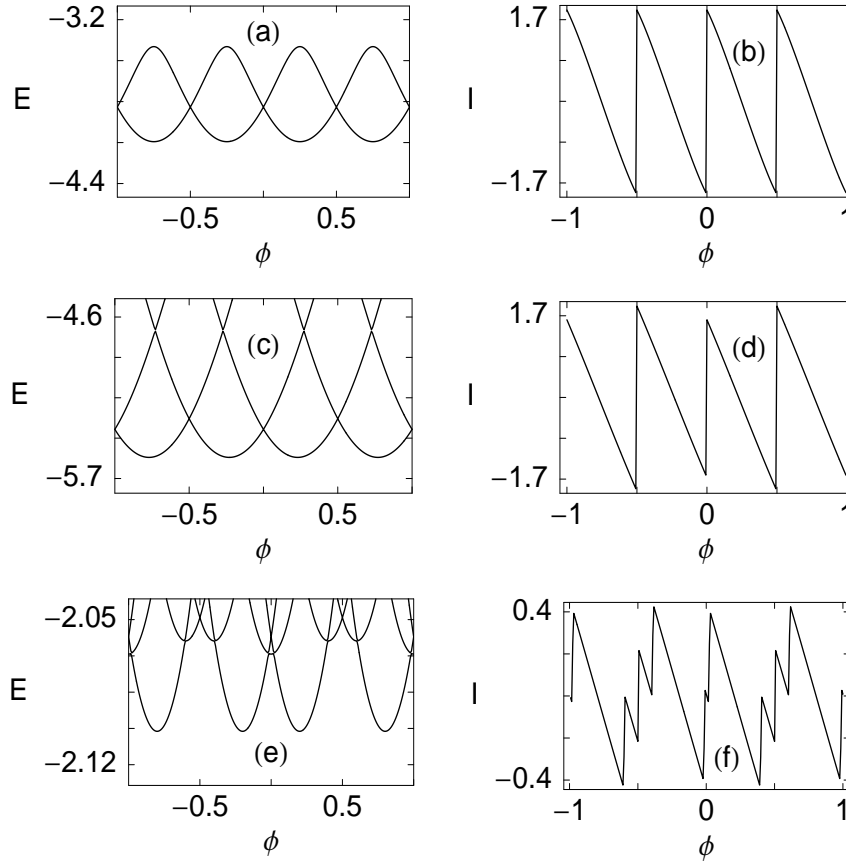
Figure 3.4: The E-ϕ and I-ϕ characteristics of the following five $(\uparrow,\uparrow,\uparrow,\downarrow,\downarrow)$ electron systems: (I) $N = 5$, $U = 2$ in (a) & (b); (II) $N = 6$, $U = 2$ in (c) & (d); and (III) $N = 6$, $U = 120$ in (e) & (f).

Rings with Three Up and Three Down Spin Electrons

Finally, we take six electron systems and study the nature of the persistent current in rings with three up and three down spin electrons. At half-filling (a benzene-like ring with $N = 6$ and $n = 6$), we see that the current becomes a continuous function of the flux ϕ as plotted in Fig. 3.5(b), exactly similar to the half-filled four electron case. The E-ϕ and I-ϕ curves for a typical non-half-filled ring with $N = 7$ and $n = 6$ are plotted in Fig. 3.5(c) and Fig. 3.5(d) respectively. Here we find striking similarity in the behavior of the persistent current with other non-half-filled systems containing even number
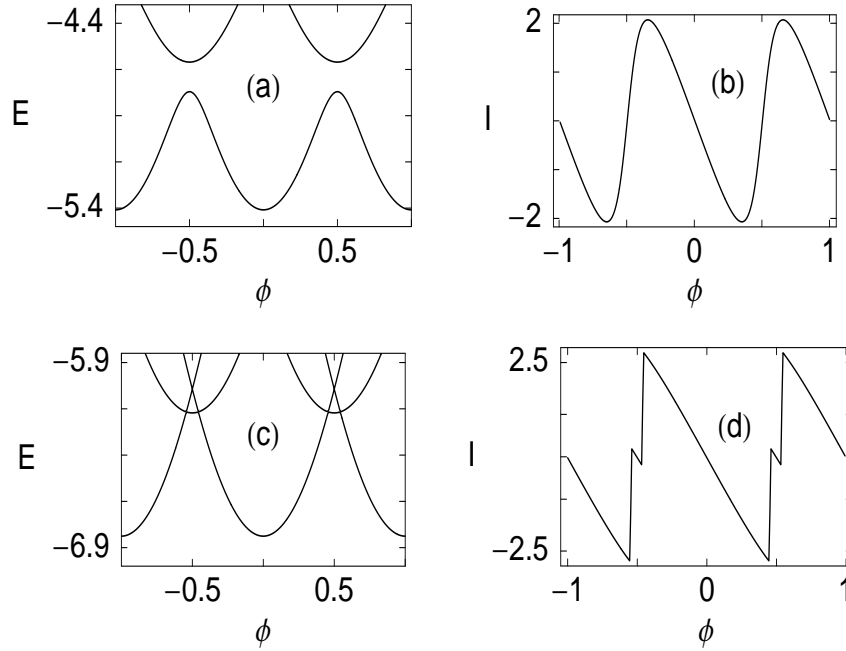
Figure 3.5: The E-ϕ and I-ϕ characteristics of the following six $(\uparrow, \uparrow, \uparrow, \downarrow, \downarrow, \downarrow)$ electron systems: (I) $N = 6$, $U = 2$ in (a) & (b) and (II) $N = 7$, $U = 2$ in (c) & (d).

of electrons. Therefore, it becomes apparent that mesoscopic Hubbard rings with even number of electrons exhibit similar characteristic features in the persistent current.

3.1.2   Drude Weight

Here we study the response of mesoscopic Hubbard rings to a uniform time-dependent electric field in terms of the Drude weight [46, 47] D, a closely related parameter that characterizes the conducting nature of the system as originally predicted by Kohn [48]. The Drude weight can be computed from the following expression [49],

$$D = \frac{N}{4\pi^2} \left[\frac{\partial^2 E_0(\phi)}{\partial \phi^2} \right]_{\phi = \phi_{min}} \tag{3.3}$$

where ϕ_{min} provides the location of the minimum of energy $E_0(\phi)$. A metallic phase will be characterized by a finite non-zero value of D, while it will be

zero in an insulating phase [48]. We plot the Drude weight D as a function of the Hubbard correlation strength U for the half-filled and the non-half-filled rings with $n = 3$, 4 and 5 in Fig. 3.6(a) and Fig. 3.6(b) respectively. For the non-half-filled rings, the number of sites corresponding to a given value of n is
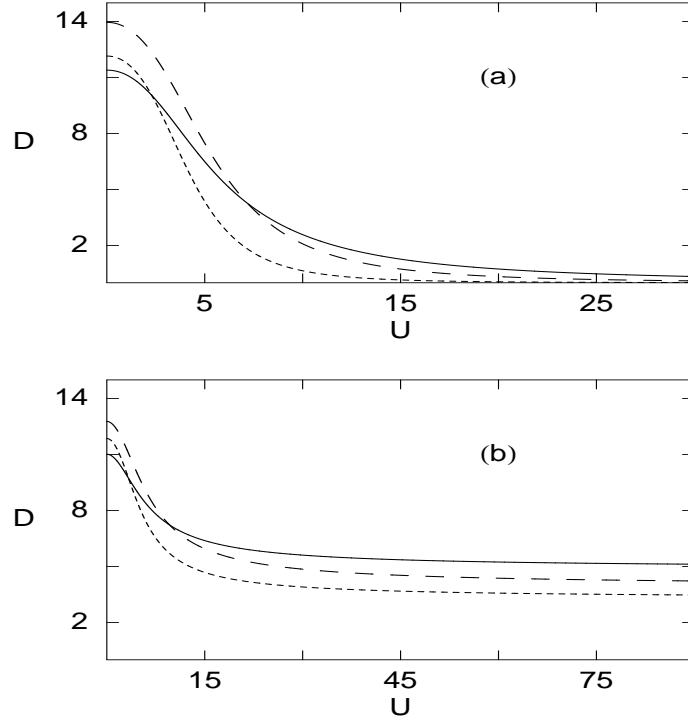

Figure 3.6: Drude weight (D) versus the Hubbard correlation strength (U) for (a) the half-filled and (b) the non-half-filled systems. The solid, dotted and dashed curves correspond to 3, 4 and 5 electron cases respectively.

taken as $N = n+1$, and we observe that the other choices of N do not affect the basic characteristics of the D-U curves. For the low values of U, the half-filled systems are in the metallic phase which is clearly evident from Fig. 3.6(a), and the systems become insulating only when the correlation strength U becomes very large. In the insulating phase ground state does not favor any empty site and accordingly, the situation is somewhat analogous to Mott localization in one-dimensional infinite lattices. On the other hand, Fig. 3.6(b) shows that the non-half-filled rings are always conducting irrespective of the correlation strength U.

Throughout our study of the persistent current in one-channel Hubbard rings without any impurity we get several interesting new results. The main results are: the appearance of kinks in persistent current, observation of both the ϕ_0 and $\phi_0/2$ periodicities in persistent currents, no singular behavior of persistent current in the half-filled rings with even number of electrons, evidence of U-independent eigenstates, existence of both metallic and insulating phases, etc. We also observe discontinuities in persistent current at non-integer values of ϕ_0 due to the electron correlation which crucially depends on the filling of the ring and also on the parity of the number of electrons. This corresponds to the anomalous Aharonov-Bohm oscillations in the persistent current with much reduced period where periodicity is not perfect, and Keyser *et al.* [45] experimentally observed similar anomalous Aharonov-Bohm oscillations in the conductance of a few-electron quantum ring.

3.2 Rings with Impurity

In order to reveal the role of disorder and electron-electron correlation on persistent current, in this section we focus our attention on certain systems which closely resemble to the disordered systems where we do not require any configuration averaging [50]. These are chemically modulated structures possessing well-defined long-range order and as specific examples we consider the aperiodic and ordered binary alloy rings. We restrict ourselves to small one-dimensional rings, as in the previous section, where persistent currents can be calculated exactly. We get many interesting new results as a consequence of the electron-electron interaction and disorder. One such promising result is the enhancement of persistent current amplitudes in these systems due to the electron correlation. This study might also be helpful to understand the physical properties of benzene-like rings and other aromatic compounds in the presence of magnetic flux ϕ.

3.2.1 Ordered Binary Alloy Rings

Here we investigate current-flux characteristics of some ordered binary alloy rings at absolute zero temperature ($T = 0$). To describe the system, we use

the tight-binding Hubbard Hamiltonian with a pure Aharonov-Bohm flux ϕ (in units of ϕ_0) without any Zeeman term. The Hamiltonian for a N-site ring becomes,

$$H = \sum_{\sigma} \sum_{i=1,3,...}^{N-1} (\epsilon_A n_{i,\sigma} + \epsilon_B n_{i+1,\sigma}) + t \sum_{\sigma} \sum_{i=1}^{N} \left(c_{i,\sigma}^{\dagger} c_{i+1,\sigma} e^{i\theta} + c_{i+1,\sigma}^{\dagger} c_{i,\sigma} e^{-i\theta} \right)$$
$$+ U \sum_{i=1}^{N} n_{i\uparrow} n_{i\downarrow} \tag{3.4}$$

where ϵ_A and ϵ_B are the site potentials for the A and B type atoms, and the other symbols of this equation carry the same meaning as described earlier. We always choose N to be even to preserve the perfect binary ordering of the
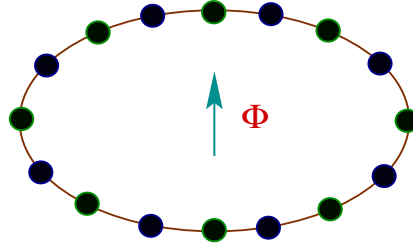

Figure 3.7: Schematic representing of a one-dimensional ordered binary alloy ring threaded by a magnetic flux ϕ. The green and blue circles correspond to two different types of atoms.

two types of atoms in the ring, as shown in Fig. 3.7.

Let us now discuss the behavior of persistent current in ordered binary alloy rings and investigate the role of electron-electron correlation on the current. In a pure ring consisting of either A or B type of atoms and in the absence of any electron correlation, the persistent current shows discontinuity at certain points of ϕ due to the ground state degeneracy and the I-ϕ curve gets a sawtooth like behavior [25]. This discontinuity completely disappears in a binary alloy ring with $U = 0$, as illustrated by the solid curve in Fig. 3.8(a). This is due to the fact that, the binary alloy configuration may be considered as a perturbation over the pure ring which lifts the ground state degeneracy and accordingly, the current $I(\phi)$ becomes a continuous function of the flux ϕ. As we switch on the electron-electron interaction, the current always decreases with the increase of the interaction strength. However, depending on the

number of electrons N_e in the ordered binary alloy rings, we get enhancement of the persistent current for the low values of U, but it decreases eventually when U becomes very large. This type of behavior is depicted in Fig. 3.8(a), where we display the current-flux characteristics for a half-filled ordered binary alloy ring with four electrons (two up and two down spin electrons). We see that for $U = 2$ (dotted line) and $U = 4$ (small dashed line), the current amplitudes
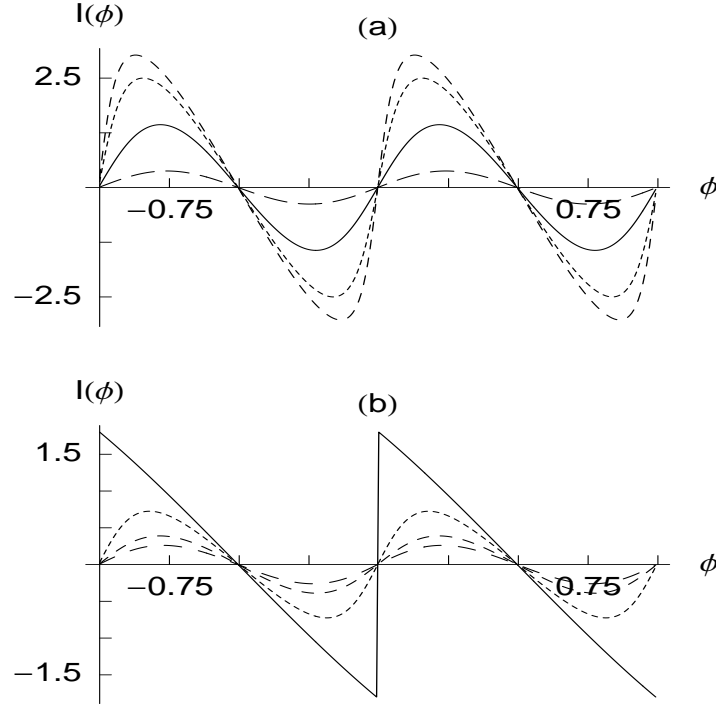

Figure 3.8: Current-flux characteristics of four $(\uparrow, \uparrow, \downarrow, \downarrow)$ electron ordered binary alloy rings, where (a) $N = 4$, $N_e = 4$ and (b) $N = 8$, $N_e = 4$. The solid, dotted, small dashed and dashed lines in (a) correspond to $U = 0$, 2, 4 and 10 respectively, while in (b) these curves represent $U = 0$, 2, 4 and 6 respectively.

are significantly larger than the non-interacting case, whereas for $U = 10$ (dashed line) the current amplitude is less than that from the $U = 0$ case. This enhancement takes place above the quarter-filling i.e., when $N_e > N/2$ and can be easily understood as follows. As N is even there are exactly $N/2$ number of sites with the lower site potential energy. If we do not take into account the electron-electron correlation, then above the quarter-filling it is

preferred that some of these lower energy sites will be doubly occupied in the ground state. As we switch on the Hubbard correlation, the two electrons that are on the same site repel each other and thus causes the enhancement of the persistent current. But for large enough U, the hopping of the electrons is strongly suppressed by the interaction and the current gets reduced. On the other hand, at quarter-filling and also below the quarter-filling, no lower
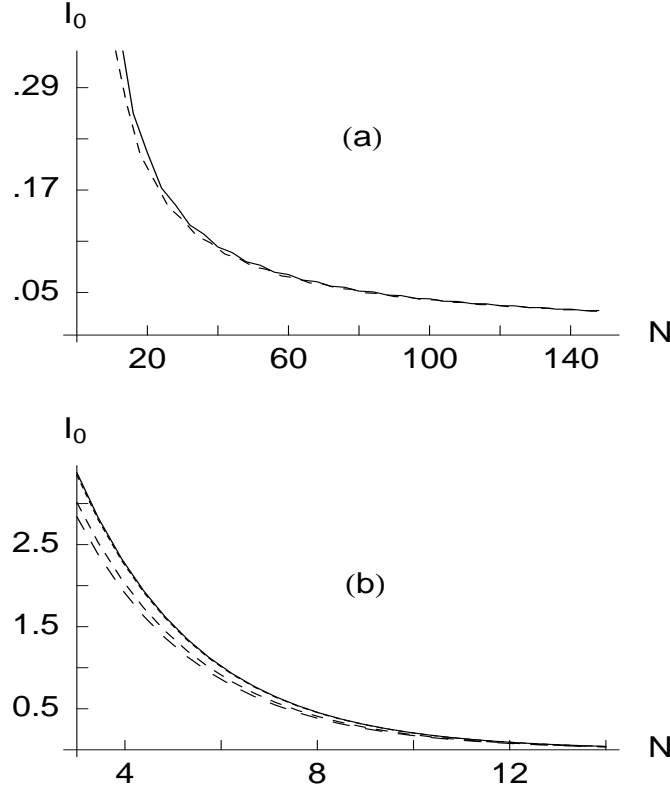

Figure 3.9: Current amplitude I_0 as a function of system size N in ordered binary-alloy rings. (a) The solid and dashed lines correspond to the non-interacting rings of size $N = 4N_e$ and $N = 4N_e + 2$ respectively. (b) The solid, dotted, small dashed and dashed lines represents the interacting rings of size $N = 2N_e$ with $U = 0.2$, 0.6, 1.5 and 3 respectively.

energy site will be doubly occupied in the ground state and hence there is no possibility of the enhancement of persistent current due to the Coulomb repulsion. In these systems we always get the reduction of persistent current with the increase of the interaction strength U. In Fig. 3.8(b), we plot the

current-flux characteristics for a quarter-filled binary-alloy ring with $U = 0$, 2, 4 and 6, and it clearly shows that the persistent currents are always suppressed by the electron correlation.

To emphasize the behavior of persistent current with system size N in ordered binary-alloy rings for the fixed electron density, we calculate the current amplitude I_0 at some typical value of magnetic flux ϕ. In Fig. 3.9, we plot I_0 as a function of the system size N for some ordered binary-alloy rings setting $\phi = 0.25$. The results for the non-interacting rings are presented in Fig. 3.9(a), where the solid and the dotted curves correspond to the rings of size $N = 4N_e$ and $N = 4N_e + 2$, respectively. Since the dimension of the Hamiltonian matrices for the interacting rings increases very sharply with N for higher number of electrons N_e, and also the computational operations are so time consuming, we present the results for the interacting rings with size $N = 2N_e$ only. In Fig. 3.9(b), the results for the interacting rings are plotted, where the solid, dotted, small dashed and dashed curves correspond to the interacting rings with $U = 0.2$, 0.6, 1.5 and 3 respectively. The curves for $U = 0.2$ and $U = 0.6$ almost coincide with each other. It is apparent from these results that, the current amplitude gradually decreases with the system size N i.e., we get a converging behavior of the current amplitude with N and most interestingly we see that, in the interacting rings the current amplitude converges to zero for any non-zero value of U. These results predict that in a realistic bulk system I_0 goes to zero as soon as the interaction is turned on.

3.2.2 Rings with Incommensurate Site Potentials

In this sub-section, we investigate persistent current in one-dimensional rings with quasi-periodic site potentials and study the effect of electron-electron interaction on persistent current. For a N-site ring with incommensurate site potentials, the tight-binding Hamiltonian can be written in this form,

$$
\begin{aligned}
H &= \sum_{\sigma}\sum_{i=1}^{N} \epsilon \cos(i\lambda\pi) c_{i,\sigma}^{\dagger} c_{i,\sigma} + t \sum_{\sigma}\sum_{i=1}^{N} \left(c_{i,\sigma}^{\dagger} c_{i+1,\sigma} e^{i\theta} + c_{i+1,\sigma}^{\dagger} c_{i,\sigma} e^{-i\theta} \right) \\
&\quad + U \sum_{i=1}^{N} n_{i\uparrow} n_{i\downarrow}
\end{aligned}
\tag{3.5}
$$

where λ is an irrational number and as a typical example we take it as the golden mean $\frac{1+\sqrt{5}}{2}$. For $\lambda = 0$, we get back the pure ring with identical site potential ϵ.

Rings with Two Opposite Spin Electrons

To investigate the precise role of electron-electron interaction on persistent current in the presence of incommensurate site potentials let us first begin our
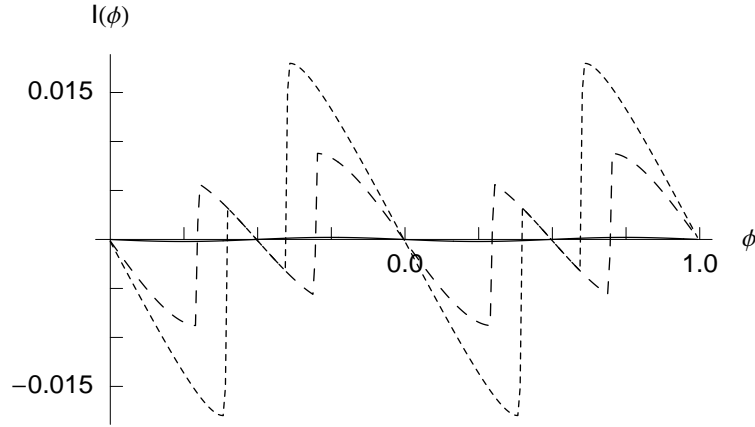

Figure 3.10: Current-flux characteristics of two $(\uparrow, \downarrow)$ electron incommensurate rings with $N = 30$. The solid, dotted and dashed curves correspond to $U = 0$, 1 and 3 respectively.

discussion with the simplest possible system which is the case of a ring with two opposite spin electrons. Fig. 3.10 shows the current-flux characteristics of a 30-site incommensurate ring, where the solid, dotted and dashed curves correspond to $U = 0$, 1 and 3 respectively. The current is highly reduced by the incommensurate site potentials in the absence of any electron correlation. This is clearly observed from the solid curve of Fig. 3.10, where it almost coincides with the abscissa. This is due to the fact that, in the presence of aperiodic site potentials the electronic energy eigenstates are critical [51, 52] which tends to localize the electrons and accordingly, the current amplitude gets reduced. But this situation changes quite dramatically as we switch on the electron-electron interaction. From Fig. 3.10 it is clearly observed that the electron correlation considerably enhances the persistent current for the low values of U (dotted

curve). This is due to the fact that the repulsive Coulomb interaction does not favor double occupancy of the sites in the ground state and also it opposes the confinement of the electrons due to localization. Therefore, the mobility of the electrons increases as we introduce the electron-electron interaction and the persistent current gets enhanced. But such enhancement ceases to occur after certain values of U due to the ring geometry, and the persistent current then decreases as we increase the correlation strength U further (dashed curve). Here we also observe that some strange kink-like structures appear in the current-flux characteristics around $\phi = \pm 0.5$ for finite values of U and the persistent currents inside these kinks are independent of the strength of the Hubbard correlation. Therefore, it reveals that the kinks appear from the U-independent energy eigenstates of these rings. The explanation for the appearance of such kinks in the persistent currents has already been discussed in our previous section for the perfect rings. In perfect rings with two opposite spin electrons, the current shows kink-like structures as long as the interaction is switched on, but in presence of the incommensurate site potentials kinks appear above some critical value of the correlation strength depending on the system size and the strength of randomness. For such two-electron incommensurate rings we get ϕ_0 periodic currents.

Rings with Two Up and One Down Spin Electrons

As representative examples of three-electron systems now we consider incommensurate rings with two up and one down spin electrons. Fig. 3.11(a) shows the current-flux characteristics for the half-filled rings ($N = 3$ and $N_e = 3$) with the correlation strength $U = 4$. In this figure, the dotted curve corresponds to a pure ring ($\lambda = 0$) which exhibits discontinuous jumps at $\phi = 0$, ± 0.5 due to the crossing of the energy levels. Quite interestingly we observe that, this pure half-filled three-electron system exhibits a perfect $\phi_0/2$ periodicity and we will see that this is a characteristic feature of the pure half-filled systems with odd number of electrons. From the solid curve of Fig. 3.11(a) it is evident that, such $\phi_0/2$ periodicity no longer exists as we introduce the incommensurate site potentials and we have the usual ϕ_0 periodicity. Moreover, in this case the current $I(\phi)$ becomes a continuous function of the flux ϕ as the

perturbation due to disorder lifts the ground state degeneracy at the crossing points of the energy levels. The characteristic features of the persistent currents are quite different in the non-half-filled rings with two up and one down spin electrons. Fig. 3.11(b) shows the results for a 12-site ring with incommensurate site potentials, where the solid, dotted and dashed curves correspond
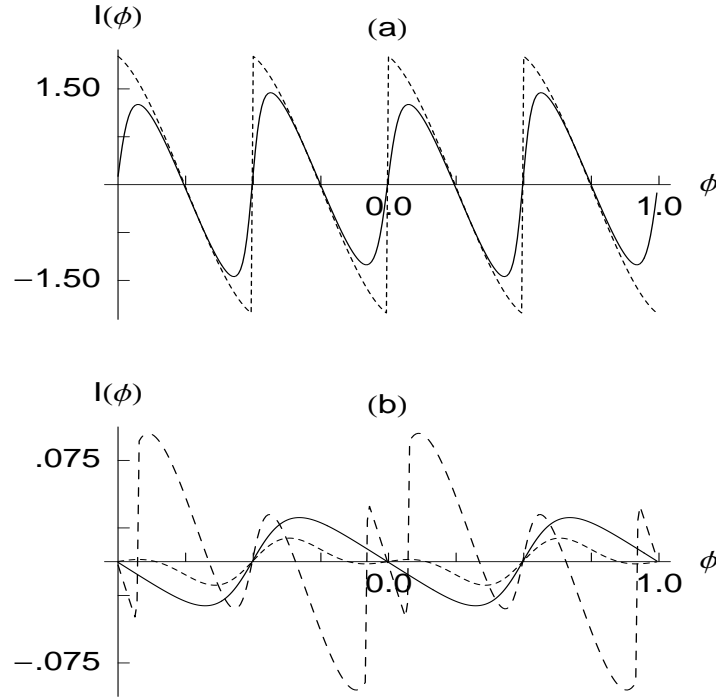

Figure 3.11: Current-flux characteristics of three $(\uparrow, \uparrow, \downarrow)$ electron incommensurate rings. (a) Half-filled $(N = 3)$ rings with $U = 4$, where the dotted and solid curves correspond to $\lambda = 0$ and $\lambda \neq 0$ respectively. (b) Non-half-filled $(N = 12)$ rings with $\lambda \neq 0$, where the solid, dotted and dashed curves represent $U = 0$, 4 and 50 respectively.

to the current-flux characteristics for $U = 0$, 4 and 50 respectively. The role of the Hubbard correlation on persistent current in presence of the incommensurate site potentials becomes evident from these characteristics curves. For the low values of U, the I-ϕ curve resembles to that for the non-interacting case and the persistent currents do not show any discontinuity. But for the large enough U, kink-like structures appear in the current-flux characteristics

as plotted in Fig. 3.11(b) by the dashed curve e.g., around the point $\phi = 0$. In this case also the kinks are due to the U-independent eigenstates like the two electron systems, and as explained earlier the currents inside the kinks are independent of the strength of the correlation U. It is observed that the persistent currents always have the ϕ_0 periodicity in the non-half-filled systems. Here we also notice that for the half-filled systems, the current always decreases with the increase of U, while in the non-half-filled rings the current gets significant enhancement due to interplay between the electron correlation and the incommensurate site potentials.

Rings with Two Up and Two Down Spin Electrons

Next we study the behavior of persistent currents in four-electron systems with incommensurate site potentials and as illustrative examples we consider rings with two up and two down spin electrons. In Fig. 3.12(a), we plot the current-flux characteristics for half-filled rings ($N = 4$ and $N_e = 4$), where the solid, dotted and dashed curves are for the cases with $U = 0$, 4 and 10, respectively. From these curves it is clearly observed that the current amplitude gradually decreases with the increase of the interaction strength U. This reveals that in the half-filled systems, the mobility of the electrons gradually decreases with the increase of U, and we see that for the large enough U, the half-filled system goes to an insulating phase. This kind of behavior holds true for any half-filled system, because at large enough U every site will be occupied by a single electron and the hopping of the electrons will not be favored due to strong electron-electron repulsion. Fig. 3.12(b) displays the current-flux characteristics for non-half-filled four-electron systems with the aperiodic Harper potential. The solid and the dotted curves are the I-ϕ curves for a 8-site ring with $U = 4$ and $U = 10$ respectively. This figure depicts that for the low values of U the persistent current $I(\phi)$ has no discontinuity but kinks appear in the I-ϕ curve at large value of U. These kinks appear at sufficiently large value of U due to additional crossing of the ground state energy levels as we vary ϕ. It may be noted that, in the present case kinks are due to the U-dependent states and not from the U-independent states as in the previous two- and three-electron cases. Both for the half-filled or the
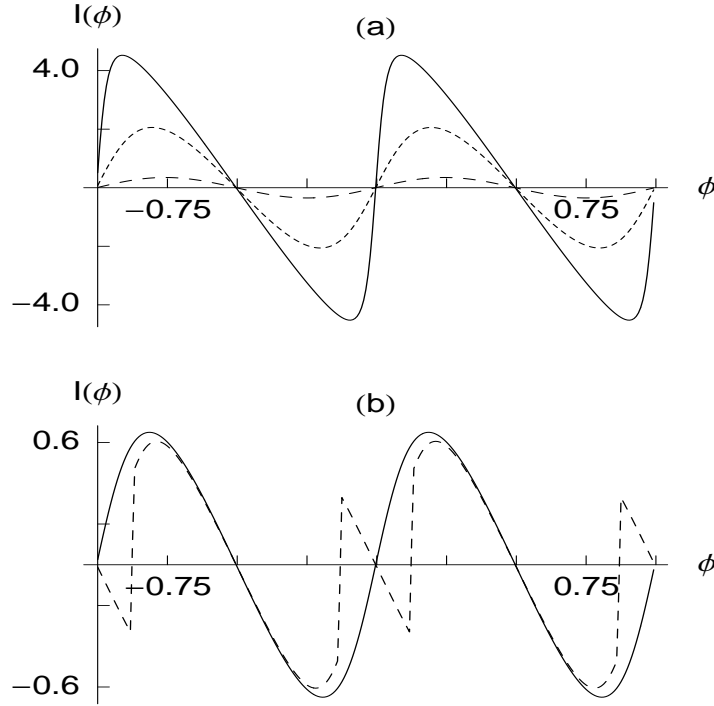
Figure 3.12: Current-flux characteristics of four $(\uparrow, \uparrow, \downarrow, \downarrow)$ electron incommensurate rings. (a) Half-filled $(N = 4)$ systems. The solid, dotted and dashed lines correspond to $U = 0$, 4 and 10 respectively. (b) Non-half-filled $(N = 8)$ systems. The solid and dashed lines are respectively for $U = 4$ and 16.

non-half-filled incommensurate rings with four electrons, we observe that the persistent currents always exhibit ϕ_0 periodicity.

Rings with Three Up and Two Down Spin Electrons

Finally, we take five-electron aperiodic rings and evaluate persistent currents in rings with three up and two down spin electrons. In pure half-filled ring $(N = 5, N_e = 5$ and $\lambda = 0)$, we get $\phi_0/2$ periodicity in the persistent current and we have already observed such period halving in other pure half-filled systems with odd number of electrons (*e.g.*, $N = 3$, $N_e = 3$ and $\lambda = 0$). Like the three-electron half-filled incommensurate rings, also in this case the ϕ_0 periodicity of the persistent current is restored once we introduce the incommensurate site potentials. The current-flux characteristics for the non-half-filled five-electron

rings with $N = 7$ are shown in Fig. 3.13. The solid and the dotted curves correspond to the rings with $U = 18$ and $U = 120$ respectively. Like as in the non-half-filled three-electron system, here also kinks appear in the I-ϕ curves above some critical value of U. Another important observation is that for large U ($U = 120$), the maximum amplitude of the current remains finite. This is
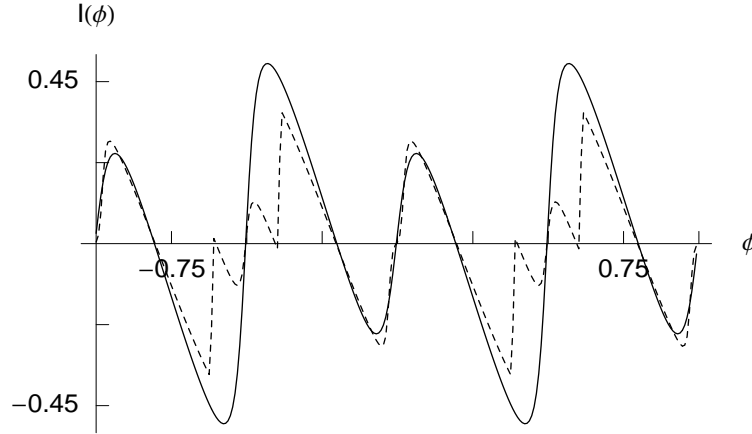

Figure 3.13: Current-flux characteristics of five $(\uparrow, \uparrow, \uparrow, \downarrow, \downarrow)$ electron incommensurate rings. The curves are for the non-half-filled ($N = 7$) rings. The solid and dotted curves correspond to $U = 18$ and 120 respectively.

quite natural since we are considering the systems with $N > N_e$, where some sites are always empty so that the electrons can hop to the empty site and thus the system always remains in the conducting phase. We also see that in these non-half-filled five-electron rings the persistent currents always have the ϕ_0 periodicity.

Now we address the behavior of persistent current with system size N for the constant electron density i.e., keeping N_e/N as a constant in the rings with incommensurate site potentials. Like ordered binary-alloy rings, here we determine the current amplitude I_0 at some typical value of $\phi = 0.25$. Fig. 3.14 displays the variation of the current amplitude I_0 with the system size N. The solid and dashed curves in Fig. 3.14(a) correspond to the results for the non-interacting rings with size $N = 2N_e$ and $N = 4N_e$ respectively. On the other hand, the results for the interacting rings with size $N = 2N_e$ are shown in Fig. 3.14(b), where the solid, dotted, small dashed and dashed

curves correspond to the incommensurate rings with $U = 0.2$, 0.6, 1.5 and 6 respectively. These curves predict that the current amplitude I_0 gradually decreases with the system size N, and for the large value of N it eventually drops to zero. Thus here we also get a converging nature of the persistent
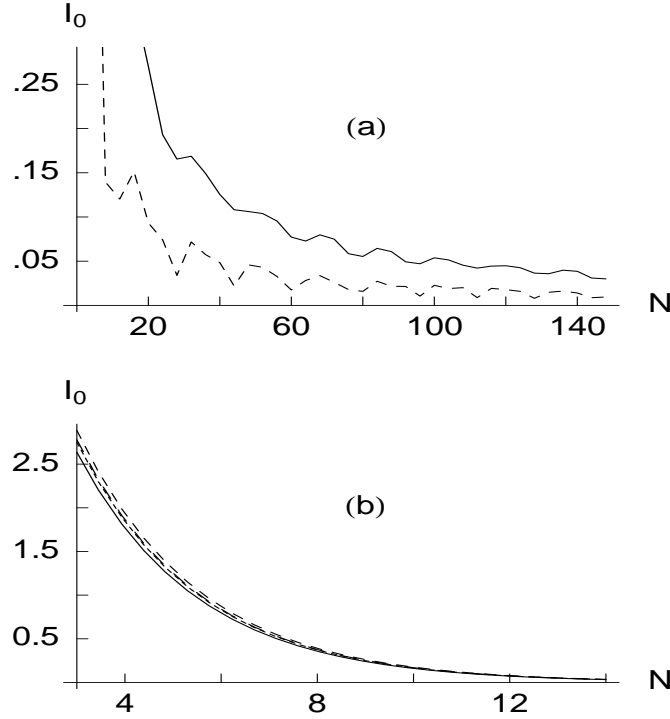

Figure 3.14: Current amplitude I_0 as a function of system size N for the rings with incommensurate site potentials. (a) Non-interacting rings, where the solid and dashed lines correspond to the rings of size $N = 2N_e$ and $N = 4N_e$ respectively. (b) Interacting rings, where the solid, dotted, small dashed and dashed lines correspond to the rings of size $N = 2N_e$ with $U = 0.2$, 0.6, 1.5 and 6 respectively.

current with the size of the ring and we can say that the current amplitude converges to zero for any non-zero value of the correlation strength for large N. From these results we can emphasize that, in a realistic bulk system I_0 vanishes as soon as the interaction is switched on.

Thus the study of persistent currents in the ordered binary alloy and the aperiodic Hubbard rings yields many interesting results due to interplay between the electron-electron interaction and the disorder in these systems. The

significant results are: (a) In the absence of electron correlation, the discontinuity in current-flux characteristics disappears due to disorder. This has been observed both in the ordered binary alloy rings and also in the aperiodic rings. (b) In pure rings with electron correlation, we observe both ϕ_0 and $\phi_0/2$ periodicities in the persistent currents. However, in the incommensurate and the ordered binary alloy rings persistent currents always have the ϕ_0 periodicity. (c) In the ordered binary alloy rings, above the quarter-filling we get the enhancement of persistent current for small values of U and the current eventually decreases when U becomes large. On the other hand, below the quarter-filling and also at the quarter-filling, persistent current always decreases with the increase of U. (d) An important finding is the appearance of kink-like structures in the I-ϕ curves of the incommensurate rings only when we take into account the electron-electron interaction. Quite surprisingly we observe that, in some cases the persistent currents inside the kinks are independent of the strength of the interaction. (e) The current amplitude gradually decreases with the system size N both for the non-interacting and the interacting rings i.e., we get a converging behavior of current with the size of the rings. Most interestingly we see that, in the realistic bulk systems I_0 vanishes as soon as the interaction is switched on. Thus the current amplitude vanishes for a ring of macroscopic size.

Chapter 4

Enhancement of Persistent Current in One-Channel Rings and Multi-Channel Cylinders

Free electron theory predicts that, at absolute zero temperature ($T = 0$), an ordered one-dimensional non-superconducting mesoscopic ring threaded by a magnetic flux ϕ supports persistent current with maximum amplitude $I_0 = ev_F/L$, where v_F is the Fermi velocity and L is the circumference of the ring. Real samples are always disordered which tends to decrease the amplitude of the persistent current, and calculations show that the disorder-averaged current $< I >$ crucially depends on the choice of the ensemble [25, 29]. The magnitude of the current $< I^2 >^{1/2}$ is however insensitive to the averaging issues and is of the order of $I_0 l/L$, l being the elastic mean free path of the electrons. This expression remains valid even if one takes into account the finite width of the ring by adding contributions from the transverse channels, since disorder leads to a compensation between the channels [25, 29].

Measurements on an ensemble of 10^7 Cu rings [18] reported a diamagnetic persistent current of average amplitude $3 \times 10^{-3} ev_F/L$ with a half flux-quantum periodicity. Such $\phi_0/2$ oscillations with diamagnetic response were also found in other persistent current experiments consisting of ensemble of isolated rings [22, 53]. The strange period-halving is due to the fact that, the first harmonic averages out to zero, while the second harmonic survives [29]. The measured average currents are comparable to the typical currents $< I^2 >^{1/2}$,

but are one or two orders of magnitude larger than the ensemble averaged currents expected from the free electron theory [25, 28, 29, 30, 31].

On the other hand, measurements on single isolated mesoscopic rings detected ϕ_0-periodic persistent currents with amplitudes of the order of $I_0 \sim ev_F/L$ (closed to the value of a perfect ring). Theory and experiment [19] seem to agree only when disorder is weak. However, the amplitudes of the currents in the diffusive single-isolated-disordered gold rings [20] were two orders of magnitude larger than the theoretical estimates. This discrepancy initiated intense theoretical activity and it is generally believed that the electron-electron correlation plays an important role in the diffusive disordered rings [33, 49, 54], though the physical origin behind this enhancement of persistent current is still unclear.

Almost all the existing theories are basically based on the framework of nearest-neighbor tight-binding model with either diagonal or off-diagonal disorder, and it has been observed that the simple nearest-neighbor tight-binding Hamiltonian cannot explain the observed enhancement of persistent current, even in the presence of electron-electron interaction. In this chapter, we will address the problem of the enhancement of persistent current in single-isolated-disordered mesoscopic one-channel rings and multi-channel cylinders, considering higher order hopping integrals in the Hamiltonian within the non-interacting electron picture, on the basis that the overlap of the atomic orbitals between various neighboring sites are usually non-vanishing, and the higher order hopping integrals become quite significant [55, 56, 57]. Physically, the higher order hopping integrals try to delocalize the electrons even in one dimension preserving their phase coherence and prevent the reduction of the persistent current due to disorder. The fluctuations in the persistent currents are also highly diminished due to the higher order hopping integrals. As a result, average amplitude of the persistent current becomes comparable to I_0 and this is exactly what has been observed experimentally.

4.1   One-Channel Mesoscopic Rings

We describe a N-site ring enclosing a magnetic flux ϕ (in units of the elementary flux quantum ϕ_0) by the following Hamiltonian in the Wannier basis,

$$H = \sum_i \epsilon_i c_i^\dagger c_i + \sum_{i \neq j} t_{ij} \left(c_i^\dagger c_j e^{i\theta_{ij}} + c_j^\dagger c_i e^{-i\theta_{ij}} \right) \tag{4.1}$$

where ϵ_i's are the site energies and the phase factor $\theta_{ij} = 2\pi\phi\left(|i - j|\right)/N$. Here we take the hopping integral between any two sites i and j through the expression $t_{ij} = t \exp\left[\alpha\left(1 - |i - j|\right)\right]$, where t corresponds to the nearest-neighbor hopping (NNH) strength. Since the hopping integrals between far enough sites give negligible contributions, we consider only one higher order hopping integral in addition to the NNH integral which provides the hopping
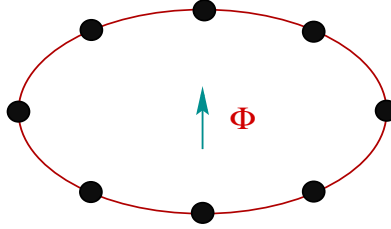

Figure 4.1: One-channel normal metal ring pierced by a magnetic flux ϕ. The filled circles correspond to the position of the lattice sites.

of an electron in the *next shortest path* between two sites. Therefore, in the case of strictly one-channel rings (Fig. 4.1) the next possible shortest path becomes the twice of the lattice spacing.

4.1.1   Impurity Free Rings

Here we study persistent currents both for impurity free mesoscopic rings described with only NNH integral, and rings described with the NNH integral in addition to the second-neighbor hopping (SNH) integral. In absence of any impurity, setting $\epsilon_i = 0$ in Eq. 4.1, the energy eigenvalue of the nth eigenstate can be expressed as,

$$E_n(\phi) = \sum_{p=1}^{p_0} 2t \exp\left[\alpha\left(1 - p\right)\right] \cos\left[\frac{2\pi p}{N}\left(n + \phi\right)\right] \tag{4.2}$$

and the corresponding persistent current carried by this eigenstate becomes,

$$I_n(\phi) = \left(\frac{4\pi t}{N}\right) \sum_{p=1}^{p_0} \exp\left[\alpha\left(1-p\right)\right] \sin\left[\frac{2\pi p}{N}\left(n+\phi\right)\right] \tag{4.3}$$

where p is an integer. We take $p_0 = 1$ and 2 respectively for the rings with NNH and SNH integrals. For large values of α, the systems described by the
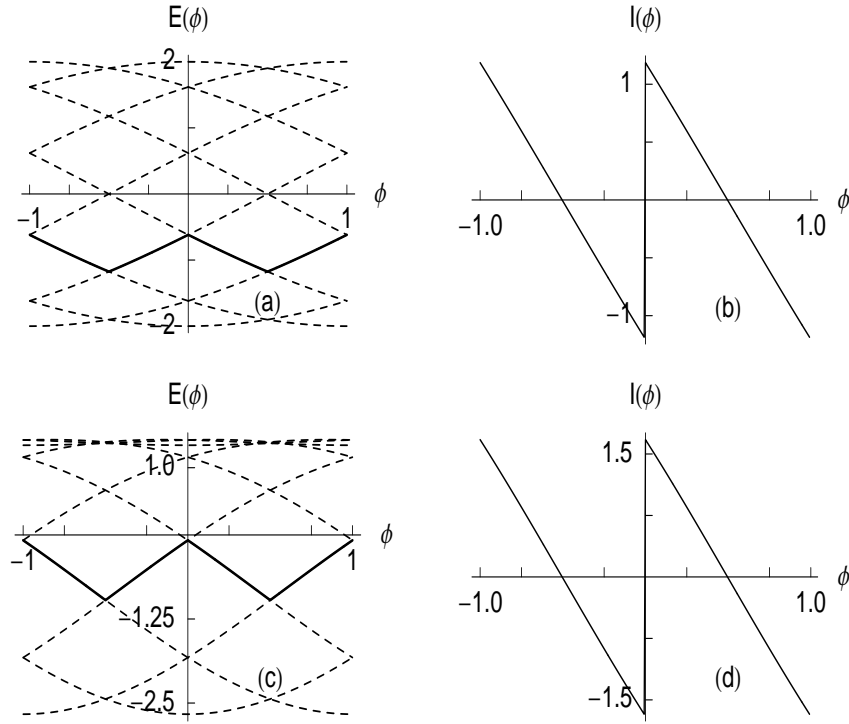

Figure 4.2: Energy spectra and the persistent currents of 10-site ordered rings with four electrons ($N_e = 4$), where (a) and (b) correspond to NNH model, while (c) and (d) correspond to SNH ($\alpha = 1.1$) model.

SNH integral eventually reduce to the systems with only NNH integral. The contributions from the SNH integral become much more appreciable only when we decrease the value of α. In such case, the energy spectrum and the persistent currents get modified and these modifications provide some interesting new results.

To have a deeper insight to the problem, let us first describe the energy spectra and the persistent currents of some small perfect rings ($N = 10$) containing four electrons ($N_e = 4$). The results are shown in Fig. 4.2. The energy

spectra for the rings described with NNH and SNH integrals are shown in Fig. 4.2(a) and Fig. 4.2(c), respectively. Here the solid curves represent the variation of the Fermi level at $T = 0$ with flux ϕ. We see that the SNH integral lowers the energy levels, and most importantly below the Fermi level
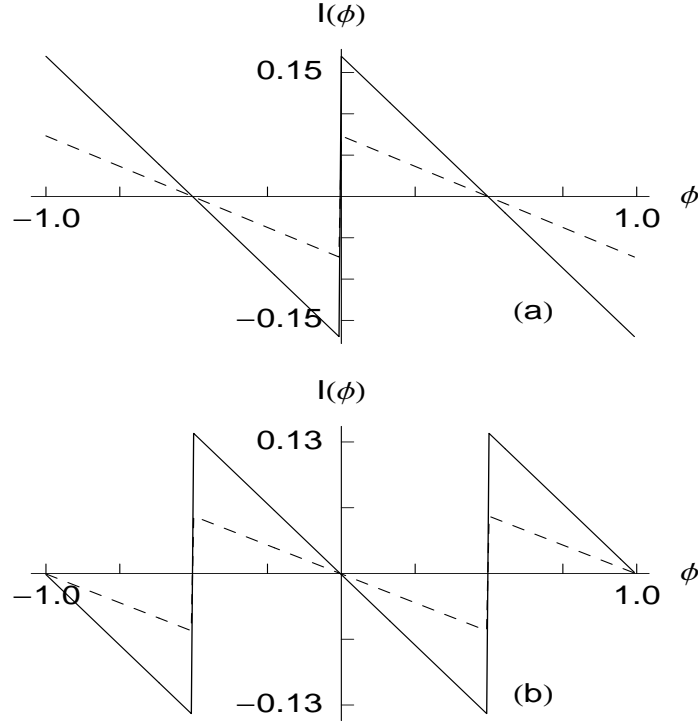

Figure 4.3: Persistent current as a function of flux ϕ for some ordered rings with $N = 100$ and $\alpha = 0.9$, where (a) $N_e = 20$ and (b) $N_e = 15$. The dotted and solid curves correspond to the rings with NNH and SNH integrals respectively.

the slopes of the $E(\phi)$ versus ϕ curves increases. As a result, the persistent current increases in the presence of SNH integrals and this enhancement of the persistent current is clearly observed from Fig. 4.2(b) and Fig. 4.2(d). In Fig. 4.2, we have considered 10-site rings only for the sake of illustration and the results for the larger rings are presented in Fig. 4.3.

In Fig. 4.3, we plot the current-flux characteristics for some perfect rings with $N = 100$ and $\alpha = 0.9$. The dotted and solid curves correspond to the variation of the persistent currents with flux ϕ for the rings described with

NNH and SNH integrals respectively. The enhancement of the current amplitudes due to the addition of SNH integral are clearly visible from Fig. 4.3(a) and Fig. 4.3(b) by comparing the results plotted by the dotted and the solid curves. Fig. 4.3(a) shows that the current has sharp transitions at $\phi = 0$ or $\pm n\phi_0$, while in Fig. 4.3(b) the current shows the transitions at $\phi = \pm n\phi_0/2$. These transitions are due to the degeneracy of the energy eigenstates at these respective fields. From Fig. 4.3 we see that, for all the above models the currents are always periodic in ϕ with ϕ_0 flux-quantum periodicity.

4.1.2 Rings with Impurity

In order to understand the role of higher order hopping integral on persistent currents in disordered mesoscopic rings, we first describe the energy spectra and the persistent currents in small rings. The results for 10-site disordered rings with $N_e = 4$ are shown in Fig. 4.4. To describe the system we use the tight-binding Hamiltonian as given in Eq. 4.1, where the site energies (ϵ_i's) are chosen randomly from a "Box" distribution function of width W. The energy spectra for the rings described with NNH and SNH integrals are plotted in Fig. 4.4(a) and Fig. 4.4(c) respectively. In these figures the solid curves give the location of the Fermi level. Like as in the ordered situations, the SNH integral lowers the energy levels and below the Fermi level the slopes of the $E(\phi)$ versus ϕ curves become much more than those for the NNH model. Thus even in the presence of impurity, we get the enhancement of persistent current due to the SNH integral, which is observed from the results given in Fig. 4.4(b) and Fig. 4.4(d) respectively.

In Fig. 4.5, we plot the current-flux characteristics for some larger disordered rings considering $N = 100$, $\alpha = 0.9$ and the disorder strength $W = 1$. The dotted and solid lines in this figure correspond to the rings described with NNH and SNH integrals respectively. The results for the even number of electrons ($N_e = 20$) are shown in Fig. 4.5(a), while Fig. 4.5(b) represents the currents for the odd N_e ($N_e = 15$). Here the persistent currents are given for some typical disordered configurations of the ring, and in fact we observe that the qualitative behavior of the persistent currents do not depend on the specific realization of the disordered configurations. Fig. 4.5 shows that the

persistent currents for the disordered rings are always periodic in ϕ with ϕ_0 flux-quantum periodicity. In the presence of impurity, the persistent current becomes a continuous function of the magnetic flux ϕ which is clearly visible from this figure (Fig. 4.5). For the perfect rings, the sharp transitions of the persistent currents at the points $\phi = 0$ or $\pm n\phi_0$ with even N_e and at
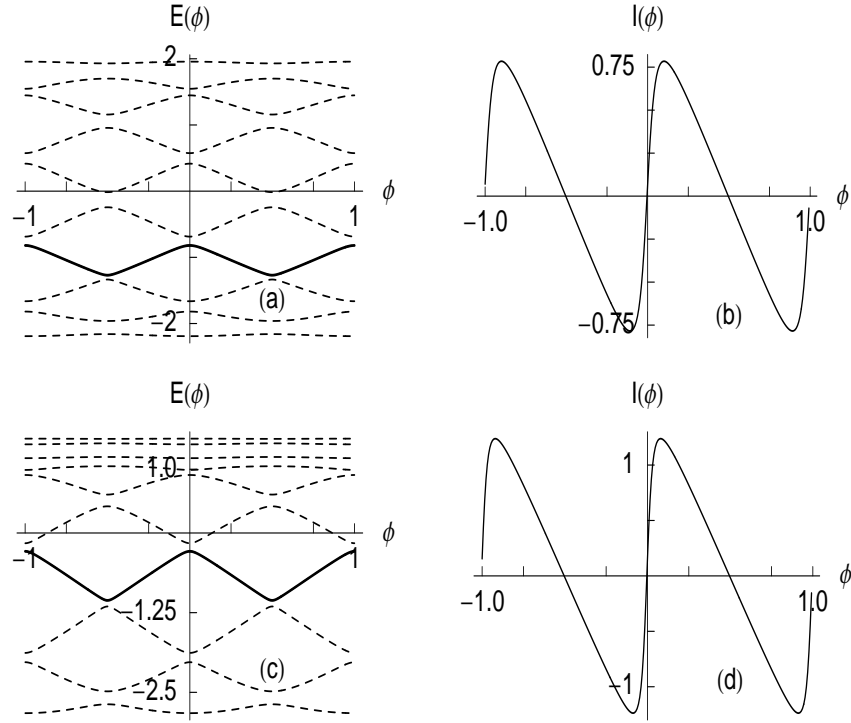

Figure 4.4: Energy spectra and the persistent currents of 10-site disordered $(W = 1)$ rings with four electrons $(N_e = 4)$, where (a) and (b) correspond to NNH model, while (c) and (d) correspond to SNH $(\alpha = 1.1)$ model.

$\phi = \pm n\phi_0/2$ with odd N_e appear due to the degeneracy of the ground state energy at these respective field points. Now as the impurities are introduced, all the degeneracies get lifted and the current exhibits a continuous variation with respect to the flux ϕ. At these degenerate points, the ground state energy passes through an extrema which in turn gives the zero persistent current as shown in Fig. 4.5. It is clear from Fig. 4.5 that, the second-neighbor hopping (SNH) integral plays a significant role to enhance the amplitude of the persistent current in the disordered rings. From Fig. 4.5(a) and Fig. 4.5(b) we

see that, the currents in the disordered rings with only NNH integrals (see the dotted curves) are vanishingly small compared to those as observed in the impurity free rings with NNH integrals (see the dotted curves in Fig. 4.3(a) and Fig. 4.3(b)). On the other hand, Fig. 4.5 shows that the persistent currents in the disordered rings with higher order hopping integral are of the same order
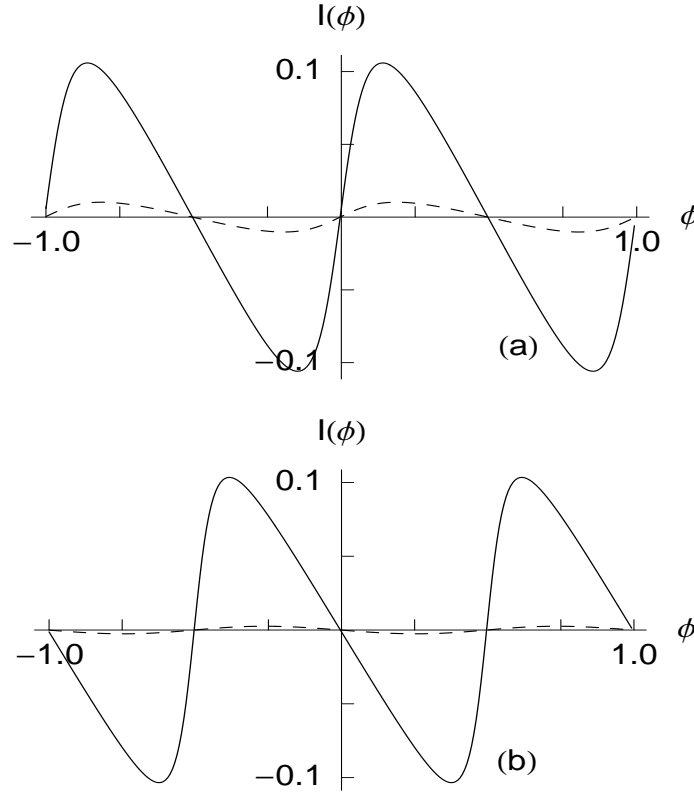

Figure 4.5: Persistent current as a function of flux ϕ for some disordered rings with $N = 100$, $\alpha = 0.9$ and $W = 1$, where (a) $N_e = 20$ and (b) $N_e = 15$. The dotted and solid curves correspond to the rings with NNH and SNH integrals respectively.

of magnitude as those for the ordered rings.

In Fig. 4.6, we plot the persistent currents for some disordered rings with higher electron concentrations, and study the cases with $N =$ even or odd and $N_e =$ even or odd. The dotted and solid curves respectively corresponds to the NNH and SNH models. It is observed that the evenness or the oddness of N and N_e do not play any important role on the persistent current, but we

will see later that the diamagnetic or the paramagnetic sign of the persistent current crucially depends on the evenness or oddness of N_e.

Physically, the higher order hopping integrals try to delocalize the electrons preserving their phase coherence and prevent the reduction of the persistent current due to disorder. In the disordered rings with only NNH integrals,
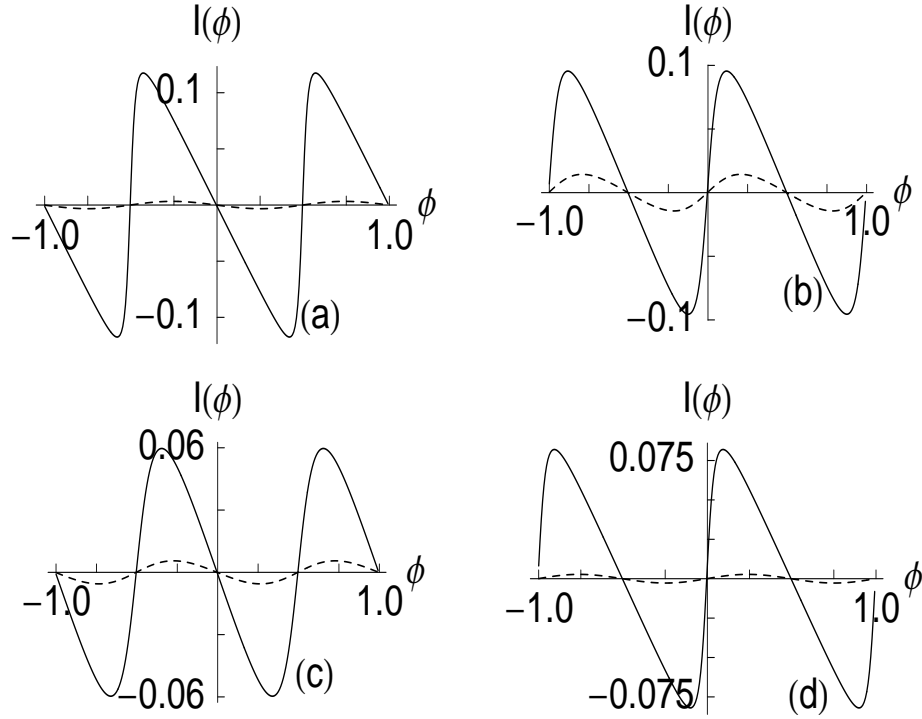

Figure 4.6: Persistent current as a function of flux ϕ for some disordered rings with higher electron concentrations and we set $W = 1$ and $\alpha = 1.1$, where (a) $N = 125$, $N_e = 45$; (b) $N = 125$, $N_e = 40$; (c) $N = 150$, $N_e = 55$ and (d) $N = 150$, $N_e = 60$.

the enormous reduction of the current amplitudes are basically due to the localization of the energy eigenstates. When we add higher order hopping integrals, it is most likely that the localization length increases and may become comparable to the length of the ring, and we get the enhancement of the persistent current.

4.2 Multi-Channel Mesoscopic Cylinders

So far we have confined our discussions only to one-dimensional systems which do not really correspond to the experimental situations. Enhancement of the persistent current has been observed even in single-isolated diffusive (disordered) metallic rings. But diffusion is not possible strictly in one dimension
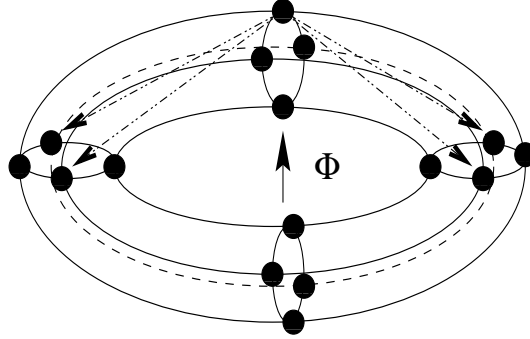

Figure 4.7: Schematic view of a multi-channel mesoscopic cylinder threaded by a magnetic flux ϕ. The filled circles correspond to the position of the lattice sites.

and it becomes necessary to consider the finite width of the samples [57]. The simplest way of doing this is to consider a cylindrical mesoscopic ring threaded by a magnetic flux ϕ. A schematic representation of the system is given in Fig. 4.7. Assuming that the lattice spacing both in the longitudinal and transverse directions are identical (i.e., the surface of the cylinder forms a square lattice), we can describe the system by the Hamiltonian,

$$H = \sum_x \epsilon_x c_x^\dagger c_x + \sum_{<xx'>} \left[t_{xx'} e^{i\theta_{xx'}} c_x^\dagger c_{x'} + t_{xx'} e^{-i\theta_{xx'}} c_{x'}^\dagger c_x \right] \qquad (4.4)$$

where ϵ_x is the site energy of the lattice point x of coordinate, say, (i, j). $t_{xx'}$ is the hopping integral between the lattice points x and x' and $\theta_{xx'}$ is the phase factor acquired by the electron due to this hopping in the presence of magnetic flux ϕ. Let us now investigate the role of just the second-neighbor hopping integral on persistent current, and neglect the effects of all the higher order hopping integrals. Let t denotes the nearest-neighbor hopping integral and the second-neighbor hopping integral (across the diagonal of the square) is taken to have the exponential form $t \exp(-\alpha)$, where α is the decay constant.

In the absence of any impurity, setting $\epsilon_x = 0$, the energy eigenvalue of the nth eigenstate can be expressed as,

$$
\begin{aligned}
E_n(\phi) &= 2t \cos\left[\frac{2\pi}{N}(n+\phi)\right] + 4te^{-\alpha} \cos\left[\frac{2\pi}{N}(n+\phi)\right] \cos\left[\frac{2\pi m}{M}\right] \\
&\quad + 2t \cos\left[\frac{2\pi m}{M}\right]
\end{aligned}
\tag{4.5}
$$

and the persistent current carried by this eigenstate is,

$$
\begin{aligned}
I_n(\phi) &= \left(\frac{4\pi t}{N}\right) \sin\left[\frac{2\pi}{N}(n+\phi)\right] + \left(\frac{8\pi t}{N}\right) e^{-\alpha} \sin\left[\frac{2\pi}{N}(n+\phi)\right] \\
&\quad \times \cos\left[\frac{2\pi m}{M}\right]
\end{aligned}
\tag{4.6}
$$

where n and m are the two integers bounded within the range $-\lfloor N/2 \rfloor \leq n < \lfloor N/2 \rfloor$ and $-\lfloor M/2 \rfloor \leq m < \lfloor M/2 \rfloor$ respectively, where $\lfloor \ldots \rfloor$ denotes the integral part. Here M and N are the number of sites along the longitudinal and transverse directions of the cylinder respectively.

Let us first describe the behavior of persistent currents in multi-channel cylinders, using the nearest-neighbor tight-binding Hamiltonian. Fig. 4.8 shows the current-flux characteristics of some mesoscopic cylinders with $N = 50$ and $M = 4$. Fig. 4.8(a) and Fig. 4.8(b) respectively corresponds to the systems with the number of electrons $N_e = 45$ and 40, where the solid curves give the currents in the absence of any impurity and the dotted curves are for the disordered systems. In the disordered mesoscopic cylinders, ϵ_x's are taken as random variables with uniform "Box" distribution of width W. The persistent current for the perfect systems (solid curves) has many discontinuities within each ϕ_0 flux-quantum period. These discontinuities are due to the existence of degenerate energy levels at certain magnetic flux, and these degeneracies get lifted as we introduce impurity into the system. Accordingly, the persistent current for the disordered systems becomes a continuous function of ϕ as shown by the dotted curves of Fig. 4.8(a) and Fig. 4.8(b). It is observed that, even in the multi-channel cylindrical systems the nearest-neighbor tight-binding model gives orders of magnitude reduction of the persistent currents compared to the results for the ballistic case.

The behavior of the persistent current for the disordered mesoscopic cylinders changes drastically as we switch on the second-neighbor hopping integrals.
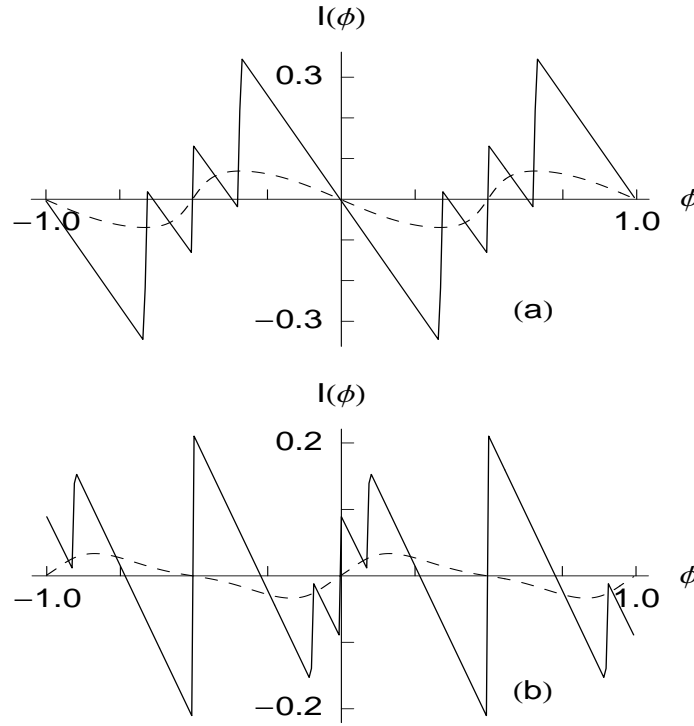
Figure 4.8: Persistent current as a function of flux ϕ for some multi-channel mesoscopic cylinders ($N = 50$ and $M = 4$) described by NNH integral only, where (a) $N_e = 45$ and (b) $N_e = 40$. The solid and dotted lines are respectively for the perfect ($W = 0$) and the dirty ($W = 1$) cylinders.

In Fig. 4.9, we plot the current-flux characteristics for some multi-channel cylinders in presence of the second-neighbor hopping integral with system size $M = 50$ and $N = 4$ taking $\alpha = 1$. The results shown in Fig. 4.9(a) and Fig. 4.9(b) are respectively for the cylinders with $N_e = 45$ and 40, where the solid and dotted lines have the same meaning as those in Fig. 4.8. From the curves plotted in Fig. 4.9(a) and Fig. 4.9(b) we see that the current amplitudes in the dirty systems (dotted curves) are comparable to that of the perfect systems (solid curves). This is due to the fact that higher order hopping integrals try to delocalize the electrons and accordingly, the current amplitudes get enhanced even by an order of magnitude in comparison with the estimates of current amplitudes in the dirty cylinders using the nearest-neighbor tight-binding Hamiltonian. This study reveals that for both the mesoscopic one-channel
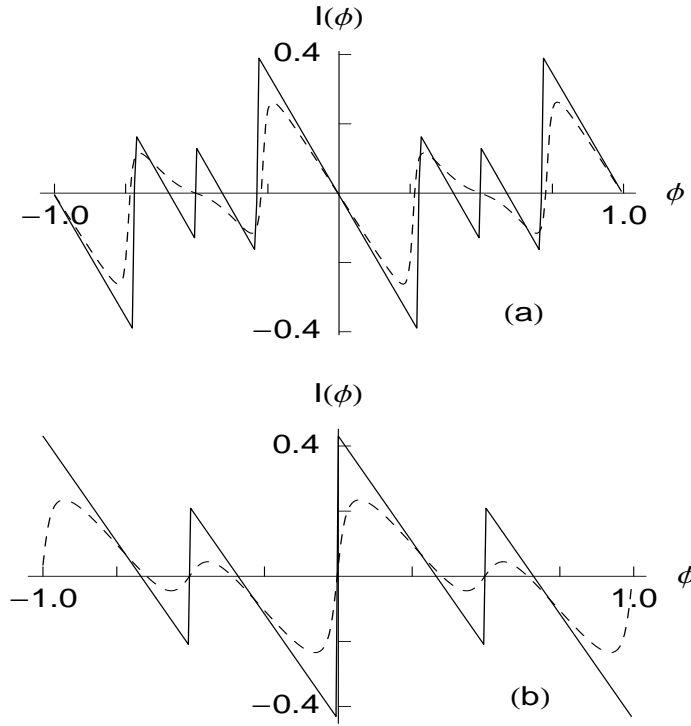
Figure 4.9: Persistent current as a function of flux ϕ for some multi-channel mesoscopic cylinders ($N = 50$ and $M = 4$) described with both NNH and SNH ($\alpha = 1.0$) integrals, where (a) $N_e = 45$ and (b) $N_e = 40$. The solid and dotted curves correspond to the perfect ($W = 0$) and dirty ($W = 1$) cylinders respectively.

rings and the multi-channel cylinders the higher order hopping integrals play a very significant role in the enhancement of the amplitude of the persistent current in disordered systems.

4.3 Variation of Persistent Current Amplitude with System Size

Here we study the variation of persistent current amplitude with system size N, and show that the higher order hopping integral plays a significant role to enhance the current amplitude in disordered mesoscopic rings and cylinders. We compute the current amplitude for different systems, keeping the ratio

N_e/N as a constant i.e., for fixed electron density. The I_0 versus N curves for one-channel rings described by the condition $N = 2N_e$ are plotted in Fig. 4.10, where we calculate the current amplitude (I_0) at some typical value of the
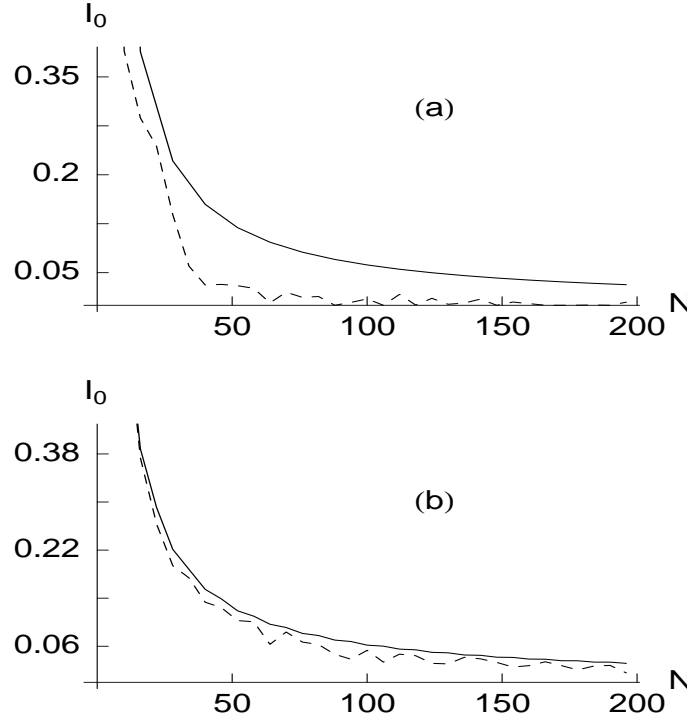

Figure 4.10: I_0 versus N curves in one-channel mesoscopic rings keeping the ratio N_e/N as a constant through the relation $N = 2N_e$, where (a) rings described with NNH integral only and (b) rings described with both NNH and SNH ($\alpha = 0.9$) integrals. The solid and dotted curves correspond to the results for the perfect and the dirty ($W = 1$) systems respectively.

magnetic flux $\phi = 0.25$. The results for the rings characterized with only NNH integral are given in Fig. 4.10(a), while Fig. 4.10(b) shows the results for the rings described with both NNH and SNH integrals. The solid and dotted curves represent the I_0-N characteristics for the rings without ($W = 0$) any impurity and with ($W = 1$) impurity respectively. In the absence of any impurity, both for the rings described with only NNH integral and the rings described with higher order hopping integral, the current amplitudes get finite non-zero value even we go for a very large value of N. On the other hand, it is

observed that for the disordered rings described with only NNH integral, the current amplitude decays very sharply (see the dotted curve of Fig. 4.10(a)) with the system size N and almost drops to zero for large N, while the current amplitude becomes comparable (see the dotted curve of Fig. 4.10(b)) to that of the perfect cases, where the rings are described with higher order hopping integral. This behavior can be physically understood as follows. In the nearest-neighbor tight-binding model, the impurity tries to localize the electron energy eigenstates and thus the phase coherence decreases gradually with the system size N. Therefore, the current amplitude decays very sharply. On the other hand, in the presence of higher order hopping integral the phase coherence length becomes comparable to that of the system size N, and we get the finite value of I_0 even for very large N.

In multi-channel mesoscopic cylinders we also get the similar kind of amplitude variation with system size N, and accordingly, in this context we do not describe these results once again.

Thus from our study of the characteristic behavior of persistent currents in mesoscopic one-channel rings and multi-channel cylinders within the tight-binding framework, we see that due to the inclusion of higher order hopping integral with the NNH model, persistent current gets an order of magnitude enhancement in the presence of impurity. Therefore, we can predict that both for mesoscopic one-channel rings and multi-channel cylinders, the higher order hopping integrals play a crucial role in the enhancement of persistent current amplitude in the presence of impurity.

Chapter 5

Low-Field Magnetic Response on Persistent Current

The diamagnetic or the paramagnetic sign of low-field persistent currents also becomes a controversial issue due to discrepancy between theory and experiment. From the theoretical calculations, Cheung *et al.* [25] predicted that the sign of persistent current is random depending on the total number of electrons, N_e, in the system and on the specific realization of the disordered configurations of the ring. Both the diamagnetic and the paramagnetic responses were also observed theoretically in mesoscopic Hubbard rings by Yu and Fowler [44]. They showed that the rings with odd N_e exhibit the paramagnetic response, while those with even N_e have the diamagnetic response in the limit $\phi \to 0$. In an experiment on 10^7 isolated mesoscopic Cu rings, Levy *et al.* [18] had reported the diamagnetic response for the low-field currents, while with Ag rings Chandrasekhar *et al.* [20] got the paramagnetic response. In a recent experiment, Jariwala *et al.* [21] have got the diamagnetic persistent currents with both integer and half-integer flux-quantum periodicities in an array of 30-diffusive mesoscopic gold rings. The diamagnetic sign of the currents in the vicinity of zero magnetic field were also found in an experiment [22] on 10^5 disconnected Ag ring. The sign of the low-field current is a priori not consistent with the theoretical predictions. In this section, we will study the nature of the low-field magnetic susceptibility of mesoscopic one-channel rings and multi-channel cylinders through some exact calculations.

The magnetic susceptibility of any mesoscopic ring/cylinder can be ob-

tained from the general expression [40],

$$\chi(\phi) = \frac{N^3}{16\pi^2} \left[\frac{\partial I(\phi)}{\partial \phi} \right] \tag{5.1}$$

Calculating the sign of $\chi(\phi)$, one can predict whether the current is paramagnetic or diamagnetic. Here we focus our attention on the systems either with fixed number of electrons (N_e) or with fixed chemical potential (μ).

5.1 One-Channel Mesoscopic Rings

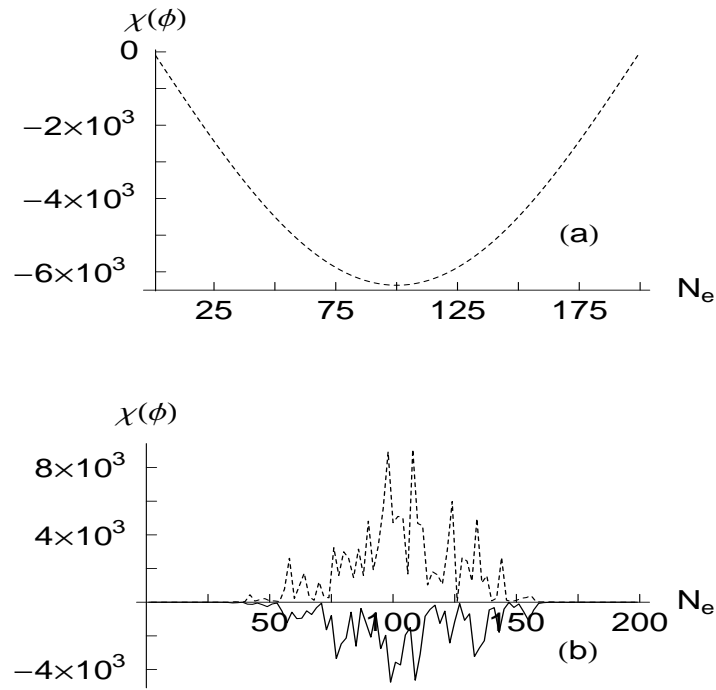Let us first study the low-field magnetic susceptibility of impurity-free one-

Figure 5.1: Low-field magnetic susceptibility as a function of N_e, for (a) perfect rings ($W = 0$) and (b) rings in the presence of impurity ($W = 1$) with $N = 200$. The solid and dotted lines in Fig. 5.1(b) correspond to the rings with odd and even N_e respectively.

channel mesoscopic rings with fixed N_e. Fig. 5.1(a) shows the variation of $\chi(\phi)$ as a function of N_e for a perfect ring with $N = 200$ in the limit $\phi \to 0$.

It is noticed that, both for the even and odd N_e the current has only the diamagnetic sign. This diamagnetic sign of the low-field currents can be easily understood from the slope of the current-flux characteristics of the one-channel impurity-free rings (see the curves plotted in Fig. 2.3). From these curves we observe that, the persistent current always exhibit negative slope at low-fields. Therefore, it can be predicted that for perfect one-channel rings the current shows only the diamagnetic sign near zero-field limit, irrespective of the total number of electrons N_e i.e., whether the rings contain odd or even N_e.

The effects of disorder on the low-field currents are quite interesting, and our results show that the sign of the currents, even in the presence of disorder, can be mentioned without any ambiguity both for the rings with odd and even N_e. In Fig. 5.1(b), we plot $\chi(\phi)$ as a function of N_e for the disordered rings. Here we take $N = 200$ and $W = 1$. The solid and dotted lines in Fig. 5.1(b) correspond to the results for the rings with odd and even N_e respectively. These curves show that the rings with odd N_e exhibit only the diamagnetic sign for the low-field currents, while for even N_e the low-field currents always have the paramagnetic sign. Physically, the disorder lifts all the degeneracies of the energy levels those were observed in a perfect ring, and as a result the sharp discontinuities of the I-ϕ characteristics (see the curves of Fig. 2.3) disappear. It may be noted that the slopes of the I-ϕ curves for even and odd N_e always have opposite signs near zero magnetic field (see the curves of Fig. 2.6). Thus for the one-dimensional disordered rings with fixed number of electrons, the sign of the low-field current is independent of the specific realization of the disordered configurations and depends only on the oddness or evenness of N_e.

5.1.1 Effect of Temperature

At finite temperature, we notice an interesting behavior of the low-field magnetic susceptibility of mesoscopic rings. Let us confine ourselves to the systems with even number of electrons. At any finite temperature, the magnetic response of these systems are always paramagnetic both for the perfect and the dirty rings in the zero field limit. For a given system, this paramagnetism is observed over a certain range of ϕ close to $\phi = 0$, say, in the domain $\phi_0/4 \leq \phi \leq \phi_0/4$. Quite interestingly we observe that, at finite temperature

the magnetic response of this particular system becomes diamagnetic beyond a critical field $\phi_c(T)$, even though $|\phi_c(T)| < \phi_0/4$.

In Fig. 5.2, we show the variation of the critical field $\phi_c(T)$ with respect to only even N_e for a perfect one-channel ring of size $N = 45$. The curve with higher values of $\phi_c(T)$ corresponds to the temperature $T/T^\star = 1.0$, while
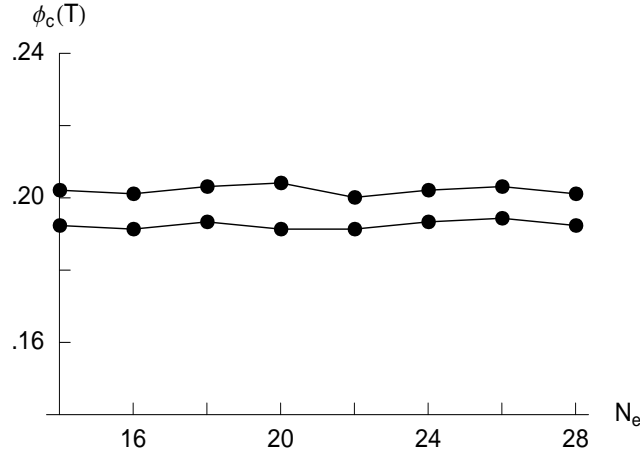

Figure 5.2: $\phi_c(T)$ versus N_e (N_e=even) curves for perfect rings with size $N = 45$.

the other curve corresponds to $T/T^\star = 0.5$. Fig. 5.3 represents the behavior of $\phi_c(T)$ for a dirty sample (with $W = 1$) at the same two temperatures $T/T^\star = 1.0$ (upper curve) and $T/T^\star = 0.5$ (lower curve). From Fig. 5.2 and Fig. 5.3 it is clear that the critical value of ϕ, where the transition from the paramagnetic to the diamagnetic phase takes place, increases with the increase of the temperature. Thus we see that, both for the perfect and dirty rings with even number of electrons there exists a critical value of magnetic flux $\phi_c(T)$, beyond which the magnetic response of the low-field currents exhibits a transition from the paramagnetic to the diamagnetic phase.

The situation is quite different even at zero temperature when we describe the system by constant chemical potential instead of fixed N_e. It may be noted that, only for some particular values of μ the system will have a fixed number of electrons, and for these values of μ the sign of the low-field currents can be predicted according to the above prescriptions. While, for all other choices of μ the total number of electrons varies even for a slight change in magnetic flux

ϕ in the neighborhood of zero flux. Hence, it is not possible to predict the sign
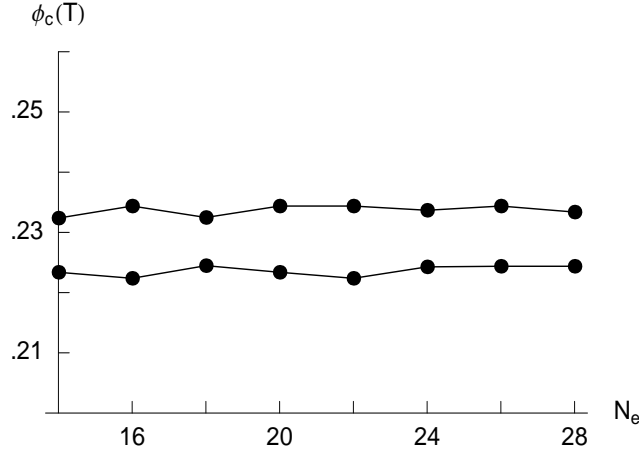

Figure 5.3: $\phi_c(T)$ versus N_e (N_e=even) curves for dirty ($W = 1$) rings with size $N = 40$.

of the low-field currents precisely, even in the absence of any impurity in the system. Thus the sign of the low-field currents strongly depends on the choice of μ, the strength of disorder and the choice of the disordered configurations.

5.2 Multi-Channel Mesoscopic Cylinders

We have also studied the low-field magnetic response for the mesoscopic rings of finite width [40]. Our study reveals that, for such systems it is not possible to predict the sign of the low-field currents precisely even for the impurity-free cases with fixed number of electrons. So we can conclude that, in the diffusive multi-channel mesoscopic rings the sign of the low-field currents is a highly unpredictable quantity as it can be easily affected by the total number of electrons N_e, chemical potential μ, magnetic flux ϕ, strength of disorder W, realizations of disordered configurations, etc. This is exactly the same picture what has been observed experimentally regarding the sign of the low-field currents.

Chapter 6

Topological Effect on Persistent Current and Sign of Low-Field Current in Moebius Strips

6.1   What is a Moebius Strip ?

A Moebius strip, also called a twisted cylinder, is a one-sided non-orientable surface obtained by cutting a closed band into a single strip giving one of the
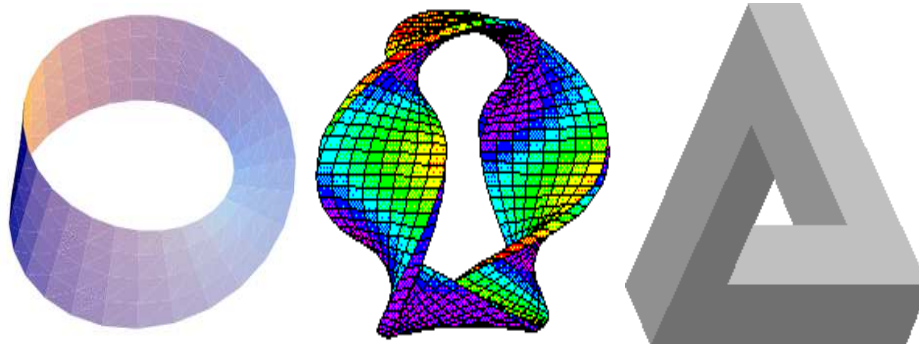

Figure 6.1: Schematic representations of different types of Moebius strips.

two ends thus produced a half-twist and then reattaching the two ends. In short, a Moebius strip has only one side and one edge. In Euclidean space, there are in fact two types of Moebius strips depending on the direction of the half-twist: clockwise and anti-clockwise. The Moebius strip is therefore chiral which is to say that it is handed. For such a twisted geometry, we get several

interesting results in the determination of persistent currents and sign of these currents in the low-field limit [58, 59, 60, 61].

6.2 Magnetic Response in Moebius Strips

In a recent experiment, Tanda *et al.* [62] have fabricated a microscopic NbSe$_3$ Moebius strip and it raises several interesting questions regarding the topological effect on magnetic response in this twisted strip geometry. Here we address the behavior of persistent current and low-field magnetic susceptibility in a Moebius strip that threads a magnetic flux ϕ. The schematic representation of such a system is given in Fig. 6.2. In the Moebius geometry,
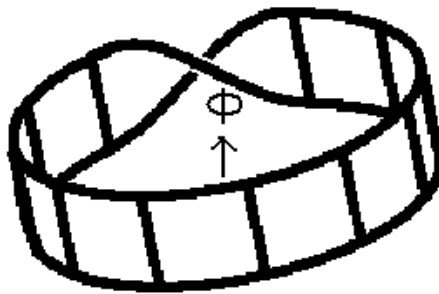

Figure 6.2: Schematic view of a Moebius strip threaded by a magnetic flux ϕ.

the motion of electrons along the transverse direction significantly affects the magnetic response which can be addressed by comparing the results with those observed in any regular multi-channel cylinder. Due to the strange geometry of the Moebius strip, it cannot be compressed into a one-dimensional structure, unlike a regular multi-channel cylinder which can be compressed into a one-dimensional ring system. Therefore, in the Moebius strip geometry if the electrons are unable to hop through the transverse direction, then an electron which travels along the ring circumference comes back to its initial position after traversing twice the path length and accordingly, it encloses 2ϕ flux. This manifests different flux periodicities in persistent currents compared to regular multi-channel cylinder.

To describe a Moebius strip with N rungs that threads a magnetic flux ϕ (in units of the elementary flux quantum $\phi_0 = ch/e$), we use the following

tight-binding Hamiltonian in the Wannier basis

$$H = \sum_{i=1}^{2N} \epsilon_i c_i^\dagger c_i + t \sum_{i=1}^{2N} \left(e^{i\theta} c_i^\dagger c_{i+1} + e^{-i\theta} c_{i+1}^\dagger c_i \right) + t_\perp \sum_{i=1}^{2N} c_i^\dagger c_{i+N} \qquad (6.1)$$

where ϵ_i's are the on-site energies and the phase factor $\theta = 2\pi\phi/N$. The parameter t denotes the nearest-neighbor hopping strength along the longitudinal direction, and the parameter $t_\perp$ corresponds to the transverse hopping strength which controls the motion of the electrons in between the two channels via the vertical bonds. In this tight-binding formulation we use the convention $c_{i+2N} = c_i$. Here we will describe all the essential features of magnetic response for the two distinct limiting cases, depending on the strength of the transverse hopping strength ($t_\perp$). One is the case where the electrons are unable to hop along the transverse direction i.e., $t_\perp = 0$, and for the other case they are allowed to hop ($t_\perp \neq 0$) along this direction.

6.2.1 Energy Spectra

In order to describe the magnetic response of Moebius strips, let us first discuss
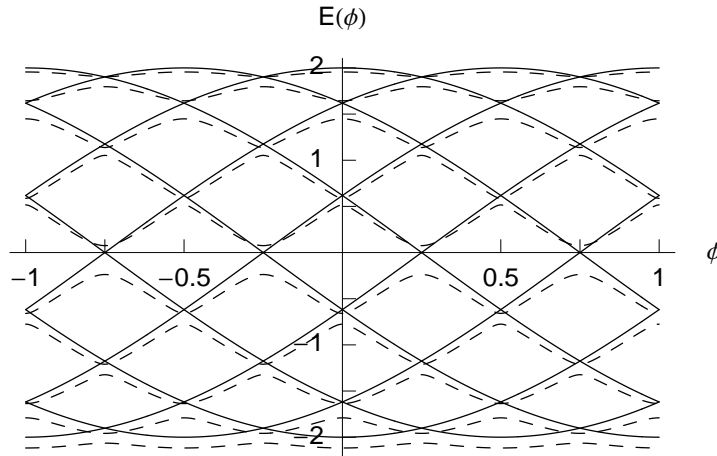

Figure 6.3: $E(\phi)$ versus ϕ curves of some Moebius strips ($N = 5$) in the limit $t_\perp = 0$. The solid and dotted curves correspond to the perfect ($W = 0$) and disordered ($W = 1$) strips respectively.

their energy-flux characteristics. The characteristic energy levels of some Moebius strips ($N = 5$) are shown in Fig. 6.3, where we fix the condition $t_\perp = 0$.

The solid and dotted curves correspond to the results for the impurity-free ($W = 0$) and disordered ($W = 1$) systems respectively. The impurities in the strip are introduced by considering the site energies from some "Box" distribution function of width W. In the absence of any impurity, the energy levels intersect with each other at different field points (see the solid curves in Fig. 6.3), while the gaps open at these intersecting points as long as the impurities are switched on (see the dotted curves in Fig. 6.3). From these E-ϕ characteristics it is observed that, the energy levels vary periodically with flux ϕ showing $\phi_0/2$ flux-quantum periodicity, instead of ϕ_0, and they have extrema at $\phi = \pm n\phi_0/4$ or $\pm n\phi_0/2$. Such half flux-quantum periodicity is not observed
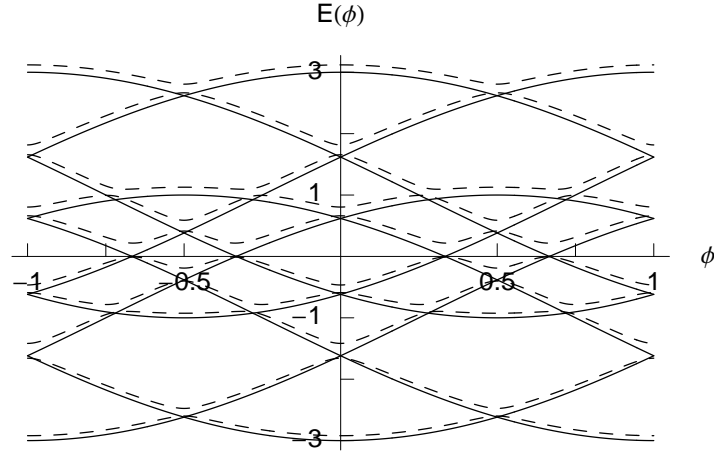

Figure 6.4: $E(\phi)$ versus ϕ curves of some Moebius strips ($N = 5$) with non-zero ($t_\perp = -1$) transverse hopping strength. The solid and dotted curves correspond to the perfect ($W = 0$) and disordered ($W = 1$) strips respectively.

in the energy spectra for regular multi-channel cylindrical systems, and it also reflects the periodicity in the determination of the persistent currents which we will describe in the forthcoming parts. Now as long as the electrons are allowed to hop along the transverse direction i.e., $t_\perp \neq 0$, one might expect effectively the similar kind of behavior of the energy spectra to that of a cylindrical strip (chapter 2). As illustrative example, in Fig. 6.4 we plot the energy-flux characteristics of some Moebius strips ($N = 5$) with non-zero transverse hopping strength ($t_\perp = -1$), where the solid and dotted curves represent the similar meaning as in Fig. 6.3. From this figure it follows that all the energy levels

vary periodically with ϕ showing ϕ_0 periodicity, as expected, instead of $\phi_0/2$.

6.2.2 Persistent Current

This section describes the current-flux characteristics for some Moebius strips those are characterized with fixed number of electrons N_e, instead of the chemical potential μ. In Fig. 6.5, we display the persistent currents as a function of ϕ for some Moebius strips ($N = 50$) in the limit $t_\perp = 0$. The solid and dotted
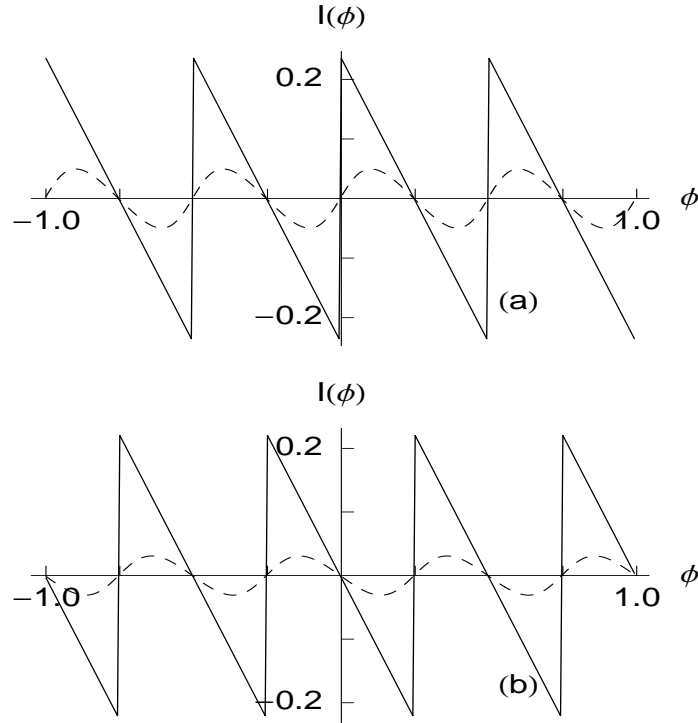

Figure 6.5: $I(\phi)$ versus ϕ curves of some Moebius strips ($N = 50$) with zero transverse hopping strength ($t_\perp = 0$), where (a) $N_e = 40$ and (b) $N_e = 35$. The solid and dotted curves represent the persistent currents for the perfect (W=0) and disordered ($W = 1$) strips respectively.

curves correspond to the currents for the perfect and disordered strips, respectively, where the results for the even number of electrons ($N_e = 40$) are shown in Fig. 6.5(a), and for the odd number of electrons ($N_e = 35$) they are plotted in Fig. 6.5(b). In the absence of any impurity, the current shows saw-tooth like behavior as a function of flux ϕ with sharp transitions at different field points.

These sharp transitions appear due to the degeneracy of the energy levels at these respective field points, which are clearly visible from the solid curves of the energy spectra given in Fig. 6.3 and Fig. 6.4. But as long as we introduce
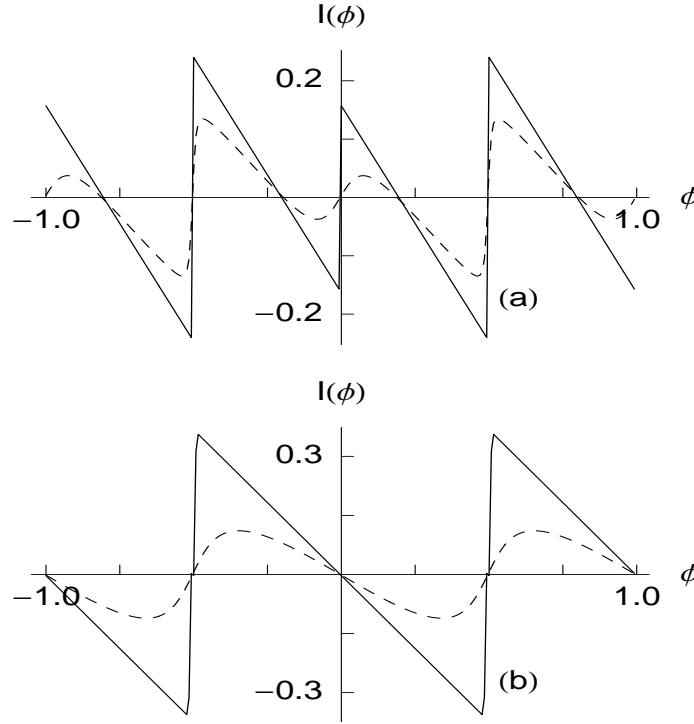

Figure 6.6: $I(\phi)$ versus ϕ curves of some Moebius strips ($N = 50$) with non-zero transverse hopping strength ($t_\perp = -1$), where (a) $N_e = 40$ and (b) $N_e = 35$. The solid and dotted lines represent the persistent currents for the perfect ($W = 0$) and disordered ($W = 1$) strips respectively.

the impurities in the system, all the degeneracies move out and accordingly, the current varies continuously as a function of ϕ and achieves much reduced amplitude. The significant observation is that, for this limit of $t_\perp$ ($t_\perp = 0$) the current shows $\phi_0/2$ flux-quantum periodicity instead of ϕ_0 which is expected from the energy-flux characteristics.

Now we focus our attention on the current-flux characteristics for the Moebius strips in which the electrons are able to hop between the transverse channels through the vertical bonds i.e., for the limit $t_\perp \neq 0$. To illustrate the results, we plot the currents in Fig. 6.6 for some Moebius strips considering

$t_\perp = -1$, keeping all the other parameters same as in Fig. 6.5. Since the electrons are able to hop along the transverse direction, the Moebius strip is expected effectively similar to that of a regular cylinder, and therefore the current shows quite similar feature as we observed in our previous chapter for the regular cylindrical systems (chapter 2). For the perfect strip with $N_e = 40$, the current shows a kink-like structure across $\phi = 0$ which is due to the additional overlap of the energy levels at this point. Several additional kinks may also appear at other field points depending on the choices of N_e and the system sizes N which we do not describe here once again. On the other hand, for the disordered systems we always get the continuous variation of the persistent current as a function of ϕ with reduced amplitude. For this limit ($t_\perp \neq 0$) the current shows ϕ_0 periodicity instead of $\phi_0/2$.

Depending on the values of the transverse hopping integral, we might also expect $\phi_0/2$ and ϕ_0 flux-quantum periodicities in persistent currents for the strips those are described by constant chemical potential μ, instead of N_e. Thus it can predicted that, both the geometrical topology and the transverse hopping strength significantly influence the flux-periodicity in the determination of persistent currents.

6.2.3   Low-Field Magnetic Susceptibility

The behavior of the low-field magnetic response is significantly influenced by the transverse hopping strength ($t_\perp$). In the limit $t_\perp = 0$, the Moebius strip becomes a one-channel system and for such a case we can estimate the sign of the low-field currents according to the prescription of a regular one-channel ring. In the absence of any impurity, the low-field current shows only the diamagnetic sign irrespective of the total number of electrons N_e i.e., whether it is odd or even. On the other hand, in the presence of impurity the low-field current shows the diamagnetic response for odd N_e, while the paramagnetic response is observed for even N_e. The key point is that the sign of the low-field currents for the disordered strip is completely independent of the specific realization of the randomness, and this behavior is exactly similar to that of a regular one-channel ring. For the other limiting case ($t_\perp \neq 0$), since the system becomes effectively identical with a regular cylindrical strip, we cannot

predict the sign of the low-field currents even in the perfect case. Since then it strongly depends on the total number of electrons N_e and also on the specific realization of the dirty strips.

Chapter 7

Concluding Remarks

In this article we have demonstrated the quantum transport properties in different types of closed loops and bridge systems. These are one-channel rings, multi-channel cylinders, Moebius strips and different types of molecular bridges.

At the beginning of this article (chapter 1), we have described very briefly some of the spectacular effects those appear in the mesoscopic systems as a consequence of the quantum phase coherence of the electronic wave functions. One of the most remarkable consequences of the quantum phase coherence is the appearance of AB oscillations in normal metal mesoscopic rings. Some other mesoscopic phenomena that were observed in mesoscopic systems are the integer and the fractional quantum Hall effects, conductance fluctuations and its quantization, etc. In this article, we have first concentrated on the spectacular mesoscopic phenomenon where a non-decaying current, so-called the persistent current, circulates in a small metallic loop threaded by a slowly varying magnetic flux. To understand the behavior of the experimental results on persistent current, one has to focus attention on the interplay of quantum phase coherence, electron-electron correlation and disorder. This is a highly challenging problem and in chapters 2-6 we have addressed this problem.

The characteristic features of persistent current in the non-interacting one-channel rings and multi-channel cylinders have been presented in chapter 2 showing its dependence on the total number of electrons N_e, chemical potential μ, randomness and the total number of channels. All the calculations have

been performed only at absolute zero temperature. In perfect one-channel rings with fixed N_e, persistent current shows saw-tooth like behavior as a function of magnetic flux ϕ with sharp discontinuities at $\phi = \pm n\phi_0/2$ or $\pm n\phi_0$ depending on whether the system has odd or even N_e. On the other hand, some additional kinks may appear in the currents for the one-channel perfect rings with fixed μ. The situation is quite different for the multi-channel perfect cylinders. In such cylindrical rings, the kinks appear in the persistent currents for both the cases with fixed N_e or fixed μ.

In chapter 3, we have explored the effects of the electron-electron correlation and disorder on persistent currents in the one-channel rings. We have used the tight-binding Hubbard model and determine persistent current by exact numerical diagonaliztion of the Hamiltonian. First, we have studied the behavior of the persistent currents in some perfect small with few number of electrons. We have obtained many interesting results those are: the appearance of kinks in the persistent currents due to electron-electron interaction, existence of both $\phi_0/2$ and ϕ_0 flux-quantum periodicities in the persistent currents, disappearance of the singular behavior of persistent current in the half-filled rings with even number of electrons, existence of the U-independent energy eigenstates, appearance of both the metallic and the insulating phases, etc. The discontinuities in the persistent current at non-integer values of ϕ_0 due to the electron correlation have also been observed, which crucially depend on the filling of the ring and also on the parity of the number of electrons. Next, we have investigated the effects of the electron-electron correlation on the persistent currents in the ordered binary alloy rings and aperiodic rings. The main results are: (a) In absence of the electron correlation both for the ordered binary alloy and aperiodic rings the discontinuity in the I-ϕ curves disappears. (b) The persistent currents exhibit only ϕ_0 flux-quantum periodicity. (c) In the ordered binary alloy rings with more than quarter-filled, we observe enhancement of persistent current for small values of U, but it eventually decreases when U becomes very large. On the other hand, below quarter-filling and at quarter-filling the current always decreases with the strength of U.

Though we have observed some enhancement of the current amplitude in the dirty rings due to electron-electron correlation, but still the amplitude is

orders of magnitude smaller than the experimentally measured values. In order to explain the enhancement of the current amplitudes, in chapter 4 we have calculated persistent currents in one-channel rings and multi-channel cylinders by including the higher order hopping integrals in nearest-neighbor tight-binding Hamiltonian, within the one electron picture. The inclusion of the higher order hopping integrals is based on the fact that the overlap of the atomic orbitals between various neighboring sites are usually non-vanishing, and these higher order hopping integrals try to delocalize the electrons and prevent reduction of the persistent current due to disorder. It has also been observed that the fluctuations of the persistent currents are also significantly diminished due to the higher order hopping integrals and the results are comparable to the experimental values.

The diamagnetic or the paramagnetic sign of the low-field currents is a controversial issue due to the discrepancy between theory and experiment. In chapter 5, we have examined the behavior of the low-field magnetic response of persistent currents by calculating the magnetic susceptibility in the limit $\phi \rightarrow 0$. In perfect one-channel rings, the low-field current exhibits only the diamagnetic sign irrespective of the parity of the total number of electrons N_e i.e, whether N_e is odd or even, while in the disordered rings currents have the diamagnetic or the paramagnetic nature depending on whether the rings contain odd or even N_e. The important point is that, for the disordered one-channel rings with fixed N_e the sign of the low-field currents is completely independent of the specific realization of the disordered configurations. In this context we have also studied the effect of finite temperature and observed that both for the perfect and the dirty rings with even number of electrons, there exits a critical value of magnetic flux $\phi_c(T)$ beyond which the magnetic response of the low-field currents makes a transition from the paramagnetic to the diamagnetic phase. But in dirty rings with constant chemical potential μ, the sign of the low-field currents cannot be predicted since it strongly depends on the choices of μ. Finally, in the case of multi-channel systems we have noticed that the sign of these currents cannot be predicted exactly, even in the perfect systems with fixed N_e as it strongly depends on the choice of N_e, μ, number of channels, disordered configurations, etc.

At the end, in chapter 6 we have discussed the topological effects on the magnetic response of a ring in a twisted geometry so-called the Moebius strip. In such systems the motion of the electrons along the transverse direction significantly affects the magnetic response. Due to the peculiar geometry of the Moebius strip it cannot be compressed into a one-dimensional structure, unlike a regular multi-channel cylinder which can be compressed into a one-dimensional ring. Therefore, we might expect different flux periodicities in the persistent currents compared to the flux periodicity as observed in regular multi-channel cylinders. Here we have considered two limiting cases depending on the value of the transverse hopping integral and observed that in the limit $t_\perp = 0$ persistent current exhibits $\phi_0/2$ flux-periodicity, while in the limit $t_\perp \neq 0$ the Moebius strip becomes a regular multi-channel cylinder. We have observed that the sign of the low-field currents can be specified in the limit of $t_\perp = 0$ only for the systems with fixed N_e, according to the prescription of a regular one-channel ring.

Bibliography

[1] S. Washburn and R. A. Webb, Adv. Phys. **35**, 375 (1986).

[2] R. A. Webb and S. Washburn, Physics Today **41**, 46 (1988).

[3] K. von Klitzing, G. Dorda and M. Pepper, Phys. Rev. Lett. **45**, 494 (1980).

[4] R. E. Prange and S. M. Girvin. *The Quantum Hall Effect.* Springer-Verlag, New York (1987).

[5] T. Chakraborty and P. Pietiläinen. *The Quantum Hall Effects.* Solid-State Sciences. Springer, Berlin, second edition (1995).

[6] Y. Imry. *Introduction to Mesoscopic Physics.* Oxford University Press, New York (1997).

[7] D. C. Tsui, H. L. Stormer and A. C. Gossard, Phys. Rev. Lett. **48**, 1559 (1982).

[8] R. B. Laughlin, Phys. Rev. Lett. **50**, 1395 (1983).

[9] A. B. Fowler, A. Hartstein and R. A. Webb, Phys. Rev. Lett. **48**, 196 (1982).

[10] P. A. Lee, A. Douglas Stone and H. Fukuyama, Phys. Rev. B **35**, 1039 (1987).

[11] D. Mailly, M. Sanquer, J.-L. Pichard and P. Pari, Europhys. Lett. **8**, 471 (1989).

[12] B. J. van Wees, H. van Houten, C. W. J. Beenakker, J. G. Williamson, L. P. Kouwenhoven, D. van der Marel and C. T. Foxon, Phys. Rev. Lett. **60**, 848 (1988).

[13] D. A. Wharam, T. J. Thornton, R. Newbury, M. Pepper, H. Ahmed, J. E. F. Frost, D. G. Hasko, D. C. Peacock, D. A. Ritchie and G. A. C. Jones, J. Phys. C: Solid State Phys. **21**, L209 (1988).

[14] J. L. Costa-Krämer, N. Garcia, P. Garcia-Mochales and P. A. Serena, Surf. Sci. **342**, L1144 (1995).

[15] Y. Aharonov and D. Bohm, Phys. Rev. **115**, 485 (1959).

[16] F. Hund, Ann. Phys. (Leipzig) **32**, 102 (1938).

[17] M. Büttiker, Y. Imry and R. Landauer, Phys. Lett. A **96**, 365 (1983).

[18] L. P. Levy, G. Dolan, J. Dunsmuir and H Bouchiat, Phys. Rev. Lett. **64**, 2074 (1990).

[19] D. Mailly, C. Chapelier and A. Benoit, Phys. Rev. Lett. **70**, 2020 (1993).

[20] V. Chandrasekhar, R. A. Webb, M. J. Brady, M. B. Ketchen, W. J. Gallagher and A. Kleinsasser, Phys. Rev. Lett. **67**, 3578 (1991).

[21] E. M. Q. Jariwala, P. Mohanty, M. B. Ketchen and R. A. Webb, Phys. Rev. Lett. **86**, 1594 (2001).

[22] R. Deblock, R. Bel, B. Reulet, H. Bouchiat and D. Mailly, Phys. Rev. Lett. **89**, 206803 (2002).

[23] M. Büttiker, Phys. Rev. B **32**, 1846 (1985).

[24] H-F Cheung, E. K. Riedel and Y. Gefen, Phys. Rev. Lett. **62**, 587 (1989).

[25] H. F. Cheung, Y. Gefen, E. K. Riedel and W. H. Shih, Phys. Rev. B **37**, 6050 (1988).

[26] R. Landauer and M. Büttiker, Phys. Rev. Lett. **54**, 2049 (1985).

[27] N. Byers and C. N. Yang, Phys. Rev. Lett. **7**, 46 (1961).

[28] F. von Oppen and E. K. Riedel, Phys. Rev. Lett. **66**, 84 (1991).

[29] G. Montambaux, H. Bouchiat, D. Sigeti and R. Friesner, Phys. Rev. B **42**, 7647 (1990).

[30] H. Bouchiat and G. Montambaux, J. Phys. (Paris) **50**, 2695 (1989).

[31] B. L. Altshuler, Y. Gefen and Y. Imry, Phys. Rev. Lett. **66**, 88 (1991).

[32] A. Schmid, Phys. Rev. Lett. **66**, 80 (1991).

[33] M. Abraham and R. Berkovits, Phys. Rev. Lett. **70**, 1509 (1993).

[34] A. Müller-Groeling and H. A. Weidenmuller, Phys. Rev. B **49**, 4752 (1994).

[35] I. O. Kulik, Physica B **284**, 1880 (2000).

[36] P. A. Orellana, M. L. Ladron de Guevara, M. Pacheco and A. Latge, Phys. Rev. B **68**, 195321 (2003).

[37] S. K. Maiti, *Anomalous quantum diffusion in order-disorder separated double quantum ring: Persistent current, Drude weight and related issues*, J. Comput. Thoer. Nanosci. (in press).

[38] S. K. Maiti, *Fractional periodic persistent current in a twisted normal metal loop: an exact result*, J. Comput. Thoer. Nanosci. (in press).

[39] S. K. Maiti, *Persistent current in one-dimensional non-superconducting mesoscopic ring: effects of single hopping impurity, in-plane electric field and foreign atoms*, IJMPB (in press).

[40] S. K. Maiti, Physica E **31**, 117 (2006).

[41] P. A. Lee and T. V. Ramakrishnan, Rev. Mod. Phys. **57**, 287 (1985).

[42] V. E. Kravtsov and B. L. Altshuler, Phys. Rev. Lett. **84**, 3394 (2000).

[43] S. K. Maiti, J. Chowdhury and S. N. Karmakar, Phys. Lett. A **332**, 497 (2004).

[44] N. Yu and M. Fowler, Phys. Rev. B **45**, 11795 (1992).

[45] U. F. Keyser, C. Führner, S. Borck and R. J. Haug, Phys. Rev. Lett. **90**, 196601 (2003).

[46] D. J. Scalapino, R. M. Fye, M. J. Martins, J. Wagner and W. Hanke, Phys. Rev. B **44**, 6909 (1991).

[47] D. J. Scalapino, S. R. White and S. Zhang, Phys. Rev. B **47**, 7995 (1993).

[48] W. Kohn, Phys. Rev. **133**, A171 (1964).

[49] G. Bouzerar, D. Poilblanc and G. Montambaux, Phys. Rev. B **49**, 8258 (1994).

[50] S. K. Maiti, J. Chowdhury and S. N. Karmakar, Solid State Commun. **135**, 278 (2005).

[51] M. Kohmoto, B. Sutherland and C. Tang, Phys. Rev. B **35**, 1020 (1987).

[52] A. Chakrabarti, S. N. Karmakar and R. K. Moitra, Phys. Lett. A **168**, 301 (1992).

[53] B. Reulet, M. Ramin, H. Bouchiat and D. Mailly, Phys. Rev. Lett. **75**, 124 (1995).

[54] T. Giamarchi and B. S. Shastry, Phys. Rev. B **51**, 10915 (1995).

[55] S. K. Maiti, J. Chowdhury and S. N. Karmakar, Synthetic Metals **155**, 430 (2005).

[56] S. K. Maiti, IJMPB **21**, 179 (2007).

[57] S. K. Maiti, J. Chowdhury and S. N. Karmakar, J. Phys.: Condens Matter **18**, 5349 (2006).

[58] K. Yakubo, Y. Avishai and D. Cohen, Phys. Rev. B **67**, 125319 (2003).

[59] E. H. M. Ferreira, M. C. Nemes, M. D. Sampaio and H. A. Weidenmüller, Phys. Lett. A **333**, 146 (2004).

[60] S. K. Maiti, Phy. Scr. **73**, 519 (2006); [Addendum: Phy. Scr. **78**, 019801 (2008)].

[61] S. K. Maiti, IJMPB **21**, 3001 (2007); [Addendum: IJMPB **22**, 2197 (2008)].

[62] S. Tanda, T. Tsuneta, Y. Okajima, K. Inagaki, K. Yamaya and N. Hatakenaka, Nature **417**, 397 (2002).

Acknowledgment

I acknowledge with deep sense of gratitude the illuminating comments and suggestions I have received from Prof. Sachindra Nath Karmakar during these works.